Dynamic encoding of valence by the anterior cingulate cortex in mice

Priyodarshan Goswamee[1,2*], Nilanjana Saferin[1], Kamalika Ganguly[1,2], Radha Shah[3], Jorge S. Seoane[1], Kari L. Neifer[1], Robert A. Pearce[4], and James P. Burkett[1*]

[1] Department of Neuroscience and Psychiatry, University of Toledo College of Medicine and Life Sciences, Toledo, OH, USA

[2] Department of Anatomy and Neurobiology, Virginia Commonwealth University School of Medicine, Richmond, VA, USA (current)

[3] College of Pharmacy and Pharmaceutical Sciences, University of Toledo, Toledo, OH 43606

[4] Department of Anesthesiology, University of Wisconsin-Madison, Madison, WI, USA, ORCID 0000-0002-1516-6260

* Corresponding authors:
James P. Burkett, Ph.D.
3000 Arlington Ave
Block Health Sciences #185
Toledo, OH 43614
419-383-4203
james.burkett@utoledo.edu

Priyodarshan Goswamee, Ph.D.
1101 East Marshall St.
Sanger Hall, Room 12-067A
Richmond, VA 23298
804-519-7800
Priyodarshan.Goswamee@vcuhealth.org

Abstract (250 words)

Fear is a double-edged sword: it supports survival based on learned associations between environmental cues and potential threats, but its dysregulation can lead to anxiety disorders and PTSD. Many studies have addressed the roles of the hippocampus and basolateral amygdala in the storage of the fear engram, but the role of the anterior cingulate cortex (ACC), especially during and immediately after fear acquisition, remains poorly defined. To address this gap, we longitudinally recorded ACC neuronal activity using single-photon calcium imaging in freely behaving adult male mice subjected to fear conditioning. Subjects acquired a conditioned freezing response to a tone cue (conditioned stimulus, CS) paired with light foot shocks (unconditioned stimulus, US), and ACC activity was monitored during cue pre-exposure, fear acquisition, fear recall, and fear extinction. Consistent with known functions of the ACC, neuronal responses were modulated by the US and by the novelty of the CS and US. Critically, both the number of CS-responsive neurons and the CS-associated population activity rose during acquisition, peaked during recall, and decreased throughout extinction. Neuronal populations responsive to the CS overlapped at a rate consistent with chance, suggesting that the ACC operates as a flexible integrative hub rather than containing stable engrams. Together, these findings indicate that ACC neuronal populations, but not engrams, represent novelty, pain, and the dynamic valence of a CS. Our findings are consistent with a model in which the ACC plays a role in threat appraisal and provides a learning signal that dynamically updates fear representations in other regions.

Acknowledgements

We gratefully acknowledge Shay Neufeld, Senior Director of Data Products and Analytics at Inscopix, for implementing several modifications to the IDEAS platform to facilitate the analysis of data presented in this study. We would like to thank Dr. Sarah Daniel of In Scripto (inscriptoscience.com) for scientific writing consultation on this manuscript.

Funding

UToledo Medical Student Research Program (JSS)

Author Contributions

PG and JPB designed the overall research study, including the conceptual background and experimental design. PG performed all behavioral testing, calcium imaging, data analysis, interpretation of results, and figure preparation, and wrote the initial manuscript draft. NS assisted with behavioral setup during data acquisition and performed analysis of animal behavior. KG contributed to data quality control and preprocessing under PG's supervision. RS performed histological verification and fluorescence imaging. JSS contributed to animal surgery and behavioral procedures under PG's supervision. RAP advised on calcium imaging analysis, early data processing strategies, and the interpretation of results. KLN provided experimental, administrative, and managerial support. JPB and RAP provided senior oversight, contributed to strategic interpretation of results, and guided final manuscript revisions. All authors reviewed and approved the final manuscript.

Competing Interests

The authors declare that they have no competing interests.

Data and Materials Availability

All raw data and metadata are available on Figshare (doi: TBD).

Supplementary Materials

Supplementary figures and tables can be found in the Supplemental Materials file.

Introduction

Fear memory enables learned associations between environmental cues and potential threats, and its dysregulation can lead to debilitating conditions such as anxiety disorders and post-traumatic stress disorder (1). Understanding the neurobiological substrates of fear memory is crucial for addressing these conditions. In mammals, fear memory is neuronally represented by the “fear engram”, which resides in the basolateral amygdala and hippocampus (both dorsal and ventral). The anterior cingulate cortex (ACC), a part of the prefrontal cortex (PFC) with strong synaptic connections to amygdala and hippocampus, plays a role in executive functions including prediction error (2), attention (3), and motivation (4-6), and has also emerged as a key player in processing of fear memory (7-17). Direct stimulation of the ACC in mice induces freezing responses and consolidates long-term fear memory, while transient inactivation impairs associative fear learning, underscoring its role in the acquisition of fear (10, 11, 17). Some research suggests that the ACC is exclusively involved in recall of remote memories (~30 days) (12, 18), while others suggest a broader role for the ACC, including the encoding and reconsolidation of recent contextual fear memories (19). Thus, the precise roles of the ACC in fear memory acquisition and consolidation remain obscure.

We hypothesize that the ACC plays an important role in encoding the valence of environmental cues that predict a negative consequence. In recent years, refined neurotechnology such as optogenetics, single- and two-photon calcium imaging have led to a surge in the exploration of the relationship between brain network activity and behavior. Single-photon calcium imaging in freely behaving rodents offers the opportunity to longitudinally track the activity of hundreds of neurons of a target brain region (20). Here, we present a single-photon calcium imaging study in which we performed longitudinal recording of more than two thousand ACC neurons collected from freely behaving adult male mice as they underwent a cued fear conditioning paradigm consisting of context pre-exposure, cue pre-exposure, fear acquisition, fear recall, and fear extinction. We measured ACC neural activity across the different stages of this paradigm. Collectively, these findings reveal that the ACC flexibly encodes the dynamic predictive value of threat-associated cues without forming persistent, overlapping memory engrams. This adds to our understanding of cortical function and positions the ACC as an adaptive integrator of valence and novelty. Our work offers new insights into the role of the ACC in fear memory processing and highlights potential cortical targets for interventions in trauma-related disorders.

Methods

Subjects

All experiments were approved by the Institutional Animal Care and Use Committee of the University of Toledo and were conducted as per the recommendations of the National Institute of Health guidelines for the Care and Use of Laboratory Animals. We used adult C57BL/6J mice, aged between 4-6 months, bred in our animal facility, and housed in a temperature and humidity-controlled housing facility under a 12-h light/dark cycle with *ad libitum* access to food and water. Following surgery, animals were singly housed to prevent potential injury to their implant site.

The a priori elimination criteria were (1) Implant placement outside the ACC and (2) fewer than 50 longitudinally registered neurons. Male (N=8) and female (N=3) mice underwent implant surgery as described below. By chance, all three female subjects were eliminated due to poor implant placement, leaving only male subjects. One male subject was eliminated for having too few longitudinally registered neurons, leaving N=7 males.

Surgery

To conduct single-photon calcium imaging in vivo, we intracranially injected adeno-associated viruses (AAV) that expressed GCaMP6f in excitatory cells (AAV1.CamK2a.GCaMP6f.WPRE.bGHpA; Inscopix, Mountain View, CA) into the right ACC and implanted a 1-mm (*dia.*) X 4-mm GRIN lens (Proview Integrated GRIN lens, Inscopix) over the GCaMP6f-expressing neurons in the ACC, enabling transmission of the fluorescent signal to the miniscope (nVoke 2.0, Inscopix) docked onto a magnetic base plate cemented to the animal's skull. For stereotactic AAV injection and implantation of GRIN lenses, we anesthetized (100 mg/kg ketamine and 2.5 mg/kg xylazine intraperitoneal [IP]) and mounted mice on a stereotactic frame equipped with a robotic controller (Neurostar, Sindelfingen, Germany). We maintained anesthesia with 1-2% oxygen-vaporized isoflurane (isoflurane: Covetrus, Portland, ME; isoflurane vaporizer: R583S, RWD, Shenzhen, China; oxygen concentrator: ROC-5A, RWD, Shenzhen, China) and monitored body temperature (Thermostar 69020, RWD, Shenzhen, China) for the duration of the surgery. All animals received subcutaneous injections of atropine (0.04 mg/kg) and extended-release analgesia (Ethiqa XR, 0.05 ml) at the start of the surgery to control excessive secretion and postoperative pain, respectively. We shaved and prepped the incision site with an alcohol and iodine scrub, exposed the skull via a midline incision, and treated with topical lidocaine. A small hole (1.8 mm diameter) was drilled in the skull overlying the right ACC (AP +1.0 mm, ML +0.4 mm) using a trephine bur attached to a motorized drill. Following excision of the dura, the cortex was primed via insertion of an Austin chisel (10096-16, Fine Science Tools, Foster City, CA) or aspirated up to a depth of 0.5 mm using a 27G blunt-end needle (SAI Infusion Technology, Lake Villa, IL) accompanied by continuous perfusion with ice-cold, sterile lactate Ringer’s solution. We lowered an aluminosilicate glass pipette containing the virus to the level of the right ACC at DV -1.75, -1.80, and -1.85

mm and infused 500 nl virus (titer strength: 3.35×10^{12} vg/mL) at a rate of 100 nl/min at each depth using a Neurostar-driven Injectomate, after which the injection pipette remained in place for 5 min before withdrawal. A 1-mm x 4-mm GRIN lens integrated with a baseplate (Inscopix) was lowered at 100 µm/min to the ACC above the viral injection site (AP +1 mm; ML +0.5 mm; DV 1.7 mm) and fixed in place using Metabond cement (Parkel, Edgewood, NY). A silicon adhesive (Kwik sil, World Precision Instruments, Sarasota, FL) was applied to cover the exposed section of the brain before Metabond application. All animals were administered an IP injection of 0.7-1.0 cc warm lactate Ringer's solution before waking up. Following surgery, all animals were individually housed in draft-free home cages with *ad libitum* access to enriched nourishment (Boost diet gel and sunflower seeds) and water. Animals were allowed to recover for 4 weeks and checked for expression of GCaMP6f before the commencement of behavioral habituation.

Single-photon Calcium Imaging

For Ca^{2+} imaging, GCaMP6f fluorescent signals were captured at 60 frames per second (FPS) from three focal planes (20 FPS per focal plane) using 488-nm excitation light delivered though the GRIN lens by a miniscope (nVoke 2.0, Inscopix). The light beam intensity was set between 0.7 and 0.9 mW/mm². Simultaneous recording of Ca^{2+} signals, animal behavior, and delivery of the stimuli were coordinated between the Inscopix Data Analysis Software (Inscopix), the nVision behavioral recording system (Inscopix), and the Freezeframe software (Actimetrics, Wilmette, IL) via Transistor-to-Transistor Logic (TTL) pulses.

Fear Conditioning

Figure 1A provides the experimental timeline and a graphical representation of the setup. Following 4 weeks of recovery from surgery, mice were prepared for the experimental procedures by being connected to the optic fiber and commutator for 3 consecutive days, during which the animal spent 5 min inside a fear conditioning chamber (Coulbourn Instruments, Allentown, PA) in a sound-attenuating chamber (Harvard Apparatus) positioned inside a second sound-attenuating cabinet (ROOM, New York, NY). Behavior was recorded using the nVision camera (Inscopix).

The following week, we recorded behavior concurrently with neuronal activity in the ACC as the mice underwent a 5-day fear conditioning protocol consisting of (day 1) a no-stimulus context pre-exposure, (day 2) cue pre-exposure, (day 3) fear acquisition, (day 4) 24-h memory (including fear recall and early extinction phases), and (day 5) 48-h memory (including extinction recall and late extinction phases). A within-session movement control period (first 300 s) was included at the beginning of every session. On the first day (context pre-exposure), mice freely explored the conditioning chamber for 15 min. On day 2 (cue pre-exposure), following 5 min of habituation, subjects were pre-exposed to five presentations of the conditioned stimulus (CS), which consisted of a neutral tone cue (30 s, 6000 kHz, 85 dB, 2-min inter-trial interval). On day 3 (fear acquisition), subjects experienced the same protocol as day 2 except that the

unconditioned stimulus (US), consisting of a mild foot shock (0.8 mA, 0.5 s), was delivered 29.5 s after the onset of each tone. On both days 4 and 5, subjects were placed in the conditioning chamber and then, after 5 min, re-exposed to 15 presentations of the same tone at 30-s inter-trial intervals. The first five tones on day 4 were used to evaluate fear recall; the first five tones on day 5 were used to evaluate extinction recall; and the last five tones on days 4 and 5 were used to evaluate fear extinction.

Conditioned freezing was assessed by quantifying mouse freezing behavior following tone onset on days 2 through 5. Behavioral analysis was performed offline using Ethovision XT 16 (Noldus), which created an annotated behavior trace with two defined states: “Freezing” and “Mobile.” Freezing bouts were defined operationally as movement below a threshold of 0.01% for longer than 1 s. Technical issues prevented data collection for one subject during the second extinction session. Additionally, only a partial dataset (limited to the first three tones) was available from the cue pre-exposure session for another subject.

Histology

At the end of behavioral experiments, animals were euthanized by isoflurane overdose followed by exsanguination via transcardial perfusion. Perfusion was performed using PBS followed by ice-cold 4% paraformaldehyde (PFA) solution. The brains were removed and submerged into 4% PFA for another 24 h at 4°C. Fixed brains were then transferred into a 30% sucrose solution. After sinking to the bottom of the storage container, the brains were embedded into plastic molds with OCT gel, rapidly frozen using dry ice, and stored at -80°C. The frozen tissue blocks were later sectioned using a cryostat (CM3050S, Leica Microsystems, Wetzlar, Germany). Coronal sections (40-µm) containing the ACC were mounted on Superfrost+ glass slides using Vectashield mounting medium and imaged using a fluorescent microscope with 4X magnification. Imaged sections were overlaid on top of an online mouse brain coronal atlas (http://labs.gaidi.ca/mouse-brain-atlas/) to confirm the position of the implanted lens and GCaMP6f expression.

Primary Processing of the Calcium Imaging Dataset

The miniscope movies were initially processed using the Inscopix data processing system (IDPS Version 1.8). The Ca^{2+} imaging movie files from three focal planes were spatially and temporally downsampled by a factor of two to generate movie files (320 *X* 198 pixels, 10 Hz frame rate). The movies were further processed using a Gaussian filter and motion-corrected for neuron identification. The Constrained Nonnegative Matrix Factorization for microendoscopic data (CNMFe) algorithm (21) was used to extract the spatial footprints of the neurons. For CNMFe, when searching for new cell seeds, we set minimums to 0.8 correlation of a pixel with its immediate neighbors, 10 signal-to-noise ratio (SNR), and 10-µm cell diameter. Multiplane registration of the coordinates of the seed pixel positions was utilized to obtain a single

cell set containing every neuron from all three focal planes. The change in GCaMP6f fluorescence over time was computed and represented as ΔF/F traces, which were further analyzed using the Inscopix Data Exploration, Analysis, and Sharing (IDEAS) Platform. Positive deflections in the ΔF/F traces that showed a fast increase in amplitude followed by a long decay back to baseline level were identified by the software as putative Ca^{2+} events. The default value of the event's smallest decay time was set at 0.2 s, as measured from the response of GCaMP6f corresponding to one action potential, as established by others (22). The threshold used to screen for events was empirically determined and set at 6x standard deviation. Raw traces were examined individually and accepted as a cell if the corresponding neurons showed activity >0.1 Hz and cell diameter between 5 and 30 µm. Timestamps of the Ca^{2+} events were synchronized with the annotation of behavioral states (mobile or freezing) generated by Ethovision XT software.

Data Analysis and Statistics

Neural circuit correlations: We used this analysis to evaluate the synchronicity of firing during the first 10 s after the onset of an event or series of events (tones or behavior states) and to compare between sessions or between behavior states. We computed the neural activity, performed a pairwise correlation of firing activity of all the neurons, and generated a correlation matrix using the Compare Neural Circuit Correlations Across States algorithm (ver. 2.1.6) of the IDEAS package. The data points were reorganized using hierarchical clustering to generate a heat-map in which groups of highly correlated neuron pairs were next to each other. The diagonal entries in the correlation matrices were set to zero. We computed the maximum correlation and generated a cumulative distribution function (CDF) for each behavior state or session. Pairwise cell–cell correlation values were compared to a reference distribution ("Other") computed from non-event-aligned neural activity windows across the session. These windows were selected to exclude stimulus-associated epochs, providing a baseline for spontaneous or background correlation levels. Within-session comparisons and effect sizes (Cohen's d) were generated using IDEAS, while between-sessions comparisons were analyzed using the Wilcoxon matched-pairs signed rank test in GraphPad Prism.

Peri-event analysis: We used the peri-event analysis algorithm (ver. 5.3.1 & 5.6.1) in the IDEAS platform, which computes the change in neural activity within a -20 s to +20 s window before and after a single event (*e.g., a* CS or US) or a series of events, to analyze the change in firing activity of both the entire population of neurons and each individual neuron and to classify them into up-modulated, down-modulated, or non-modulated sub-populations. For each analysis, a null distribution for comparison was generated by circularly permuting the event time relative to the neural time series using 1000 random shuffles, resulting in a p-value resolution of α=0.001. The neural activity Z-score of individual neurons was calculated at each time increment using the equation $Z = X - \mu/\sigma$ where X is the observed firing rate, μ is the mean firing rate, and σ is the standard deviation of the firing rate. Next, the bootstrap probability was calculated by determining the fractions of the null distribution that were greater than and

less than the observed neural activity Z-score. Two-tailed t-tests were performed, and populations/cells were labeled as up-modulated if the bootstrap probability was <α/2, down-modulated if the bootstrap probability was >1-α/2, and non-modulated if the bootstrap probability was between α/2 and 1-α/2. The Combine and Compare algorithm (ver. 2.5.1) in IDEAS combined peri-event data from two groups independently for each group. Following aggregation of data from all recordings, the proportions of up-, down- and non-modulated cells across all sessions were compared using chi-squared tests.

All accepted cells from a session were included in our analyses for within-session comparison of activity. In contrast, only the longitudinally registered (LR) cell sets were utilized to compare between sessions of interest (Fig. S1D). The event-associated population activity (EAPA) traces were then exported to Microsoft Excel to determine the peak amplitude (ΔZ_{PEAK}) and area under the curve (AUC) of the event-aligned activity traces. A 5-point moving average was applied to mean Z scores to reduce noise. The peak amplitude was defined as the difference in Z-score between the post-event maximum (from 0 to +20 s) and the average pre-event Z-score (from -20 to 0 s). The timepoints before and after the peak during which the true mean crossed the threshold (mean of shuffled Z scores) were identified as the onset and offset of the population responses, respectively. The area under the curve (AUC) was calculated by subtracting the neural activity Z-score from the pre-event Z-score at every recorded time interval, multiplying the difference by the length of the time interval, and summing these values for all intervals between onset and offset. For the purposes of calculating the AUC, the earliest possible onset was 0 s, and the latest possible offset was +20 s.

The overlap between LR neurons (N=1205) responsive to the CS and US at three timepoints (early acquisition, late acquisition, and recall) were evaluated to determine whether consistent populations were responsive across time. The expected overlap by chance for each possible pair of conditions was calculated by counting the number of responsive neurons for each condition, converting to frequencies, then multiplying the frequencies together. The observed overlap for each possible pair of conditions was determined by counting the neurons that were responsive to both conditions regardless of the direction of the responses. Observed vs. expected frequencies were compared using chi-squared tests. A smallest effect size of interest was chosen as Cohen's w=0.1, therefore defining statistical equivalence as $X^2<4.8$.

***Statistics*:** The between-sessions percentage of freezing time was compared among all subjects using mixed-effect models due to availability of partial datasets for some of the recording sessions. Post hoc comparison of freezing percentages was performed using Sidak's multiple comparison test. Within-session or between-sessions differences in peak amplitudes and AUC were evaluated using two-tailed t-tests or a one-way repeated measures ANOVA. Changes in the percentages of up-modulated, non-modulated, and down-modulated cells were evaluated within and between sessions using chi-squared tests. When chi-squared tests were used to compare observed to expected, the percentages expected by chance of up-modulated, down-modulated and non-modulated neurons were considered to be 5%, 5%, and 90%, respectively.

Results

Viral expression, lens placement, and registration of neurons.

Prior to behavioral testing, mice underwent stereotaxic surgery for the implantation of a GRIN lens and injection of a GCaMP6f-expressing viral vector targeting the right anterior cingulate cortex (ACC; Fig. 1A). Animals included in the final analysis displayed robust on-target expression of the reporter and accurate implant placement, as verified by post-mortem histological assessment (Fig. 1B). Only mice with proper alignment between the expression zone and lens placement were retained, resulting in a final cohort of 7 male mice (Fig. S1A-D). The representative animal shown throughout the manuscript is indicated by the green bar in Figs. S1A–B. Neuronal spatial footprints were extracted from calcium imaging data, multiplane registration (MPR) was performed to enable the tracking of cells across all the focal planes (Fig. 1C-E). Data processing, motion correction, event detection, and ΔF/F signal extraction were carried out using the IDEAS platform as described in the Methods. Raster plots and event timing distributions from a representative subject during the fear conditioning session are shown in Fig. 1F. The average number of accepted neurons per subject per session (mean ± SEM) were as follows: cue pre-exposure, 363 ± 85; acquisition, 323 ± 78; 24-h memory, 347 ± 56; and 48-h memory, 327 ± 56 (Fig. S1C–D). A schematic of the registration workflow is shown in Fig. S1D. For within-session analyses, all accepted neurons were included to assess cue-evoked activity. For between-session comparisons, only neurons that could be reliably tracked across two consecutive sessions (longitudinally registered cells, or LR cells) were used, enabling direct assessment of changes in the same cell population over time. As a result, neuronal datasets from Days 2–4 were each included in two separate LR pairs, one aligned with the preceding session and once with the subsequent session, and each between-sessions comparison involved a different ‘n’ of cells.

Classical fear conditioning.

Following recovery from surgery, mice were trained on a cued fear conditioning paradigm consisting of cue pre-exposure, fear acquisition, and two subsequent memory sessions (24-h and 48-h; Fig. 1A). Freezing behavior increased significantly during tone presentations in the acquisition session compared to cue pre-exposure (mixed effects model, session x tone interaction, $F(4,28)=3.8$, $p=0.014$), indicating successful acquisition of the CS–US association (Fig. 2A), with significantly higher freezing during late acquisition (Sidak’s test: tone 4, $p=0.031$; tone 5, $p=0.0011$). During the 24-h memory session, mice showed elevated freezing during recall tones relative to pre-exposure tones (t-test, $p = 0.0074$, $t=3.964$, Fig. 2B), indicating successful recall of the CS-US association. Mice maintained elevated freezing across 30 tone presentations (Fig. 2C) with no significant differences between sessions ($F(1,25)=0.37$, $p=0.55$) or across tones ($F(4,30)=0.097$, $p=0.98$), suggesting persistent fear memory and a failure to extinguish the conditioned response. Thus, mice successfully acquired and recalled a

conditioned association between the CS and US but failed to extinguish this association during the 24-h and 48-h memory sessions.

ACC population activity during mobile and freezing states.

We first investigated whether the expression of fear-related behavior corresponded to the neural activity of ACC neurons. For this, the Ca^{2+} activity traces during two sessions (acquisition and 24-h memory) were overlaid with behavioral traces that were annotated with two mutually exclusive behavioral states, freezing and moving (Supplementary Figs. S2A-B). Within-session comparison of neural activity during freezing and moving states from N=7 subjects during the acquisition (Fig. 2D) and 24-h memory (Fig. 2E) sessions detected no difference in overall ACC activity during these states (paired t-tests: moving, p=0.49, t=0.71; freezing, p=0.45, t=0.77; acquisition, N=2007 cells; 24-h memory, N=2067 cells; N=7 mice; Fig. 2F). However, a comparison of the proportions of up-, down- and non-modulated neurons between states and between sessions showed a greater proportion of up-modulated neurons in the moving state and a greater proportion of down-modulated neurons in the freezing state (X^2=157; p<0.00001; Figs. 2G-H). Although both were slightly higher during acquisition than during 24-h memory (moving: X^2=18.0, p=0.0001; freezing: X^2=17.9, p=0.0001), there were no overall between-sessions differences in neural activity among modulated neurons (Paired t-tests; moving: up, p=0.44, t=0.79; down: p=0.77, t=-0.29; freezing: up, p=0.85, t=-0.19; down, p=0.46, t=0.76; n= 2007, Supplementary Fig. S2C). This demonstrates that moving and freezing states during the acquisition and 24-h memory sessions are accompanied by changes in the proportion of modulated neurons in the ACC.

Next, we compared the neural synchrony between ACC neurons during freezing and moving by comparing the pairwise correlations of neuronal firing activity between behavioral states in the acquisition and 24-h memory sessions (Figs. 2I-J). The cumulative frequency distribution (CFD) plot shows a rightward shift accompanying freezing states in both sessions, indicating an increase in neural synchrony during freezing (acquisition: Cohen’s d=-0.35; p=0.0001; 24-h memory: Cohen's d=-0.13; p=0.0001; Fig. 2K). There were no between-sessions differences observed in the neural synchrony during these states (Wilcoxon signed rank: freezing, p<0.0001, W=-3.8×10^5; moving, p=0.0048, W=1.9×10^5, Fig. 2K).

To determine whether the onset of freezing and moving states corresponded to modulation of ACC activity independently from the CS, we compared the change in the activity of ACC neurons following the onset of freezing and moving during the first five minutes of the session, before CS presentations began (Fig. S2D). The onset of these behavioral states did not result in a significant difference in the activity of ACC neurons (AUC: p = 0.6844, t=0.4269, and Amplitude: p=0.6187, t=0.5246, n= 7) or the proportions of modulated neurons (X^2=1.4, p=0.51) (Fig. S2E-F), providing no evidence that the onsets of the freezing and moving states are associated with the modulation of neuronal activity independent of a CS. Collectively, these results provide evidence that

freezing states during a CS, but not during habituation, are represented in the ACC by an increase in the proportion of down-modulated neurons and an increase in neural synchrony.

Dynamic modulation of ACC activity by the US during fear acquisition.

Next, we analyzed how CS and US events were represented by ACC neurons across the fear conditioning paradigm, focusing on event-aligned population activity (EAPA) and the proportions of modulated neurons. Temporal changes in EAPA surrounding all shock events were measured both at the level of the full population (Figs. 3A-B; Fig. S2) and at the level of individual neurons (Fig. 3C). ACC neuronal subpopulations were significantly modulated following shock events and the proportions of both up-modulated and down-modulated neurons across all shock events were higher than expected by chance (X^2=263; p<0.00001; Fig. 3D).

To assess how ACC activity changes in response to repeated aversive stimuli, we analyzed calcium signals time-locked to each of five footshocks during the acquisition session. Differences in EAPA were evaluated using the peak response amplitude and the response magnitude, calculated by integrating the area under the curve (AUC) between peak onset and peak offset. The peak amplitude of firing activity differed significantly across shocks (ANOVA, p=0.017, F(2.3,13.9)=5.2, N =7, Fig. 3E), with a significant decrease from Shock 1 to Shock 2 (p=0.039) and trends toward further reduction (Shock 1 vs 3, p=0.054; 1 vs 4, p=0.097; 1 vs 5, p=0.16). These results suggest a rapid attenuation of novelty-driven peak ACC activity after the initial shock exposure. However, the overall response magnitude did not significantly differ across shocks (AUC: ANOVA, p=0.3196, F(2.3,13.7)=1.3; Fig. 3F). Moreover, we observed that the population of up-modulated, but not down-modulated, neurons significantly varied across the repeated footshocks (up: ANOVA, p=0.0004, F(2.8,16.6)=11.22; down: mixed effects model, p = 0.21, F(2.1,12.5)=1.8, N=7; Fig. 3G-H). Specifically, the proportion of up-modulated neurons peaked during Shock 1 and decreased during all subsequent shocks (Dunnett's test: Shock 1 vs Shock 2, p=0.0018; vs Shock 3, p=0.0020; vs Shock 4, p=0.0029; vs Shock 5, p=0.0050). There was no difference in the average change in peak firing rate across the shocks in either populations (up: ANOVA, p=0.51, F(1.9,13.5)=0.71, Fig. 3I; down: mixed effect model, p=0.52, F(2.1,13.9)=0.69; Fig. 3J). These findings show that the ACC responds to foot shocks with an increase in EAPA amplitude and more modulated neurons, and that the ACC response to foot shocks is greatest during the first shock event.

Differential activation of ACC neuronal networks encoding aversive-predictive cues.

To assess how ACC population activity in response to the CS evolved from the cue pre-exposure session to the acquisition session, we analyzed longitudinally registered (LR) neurons with all tone events averaged per session. A clear CS-aligned EAPA pattern was visible in both sessions (Fig. 4A), but a comparison of the kinetic

parameters of these EAPA traces between these sessions showed no significant differences in peak amplitude (paired t-test, p=0.54; t= 0.65, N=7; Fig. 4B) or response magnitude (AUC: paired t-test, p=0.71; t=0.39, N=7; Fig. 4C). The proportions of modulated neurons in both sessions were consistent with chance (cue pre-exposure: X^2=0.02, p=0.99; acquisition: X^2=3.9, p=0.14), with no differences between sessions (X^2=2.4, p=0.30) (Figs. 4D–E) and no significant change in the mean activity of either modulated population (paired t-tests, up-modulated: p=0.57, t=0.61, N=6; down-modulated: p=0.12, t=1.9, N=6; Fig. 4F-G). One subject had no up-modulated neurons during acquisition and was excluded from that analysis.

We next compared early and late tone responses between sessions. Early tones during cue pre-exposure evoked higher peak EAPA amplitude than during acquisition (paired t-tests, p = 0.050; t=2.4, N =7; Figs. 4H-I), though the magnitude of the responses did not reach statistical significance (AUC: paired t-test, p=0.12, t=1.8, N=7; Fig. 4J). The proportion of both up-modulated and down-modulated neurons were highest during early pre-exposure (X^2=44, p<0.00001; Figs. 4K–L). The mean response amplitudes of the two modulated subpopulations did not change significantly (paired t-tests, up-modulated: p=0.22, t=1.4, N=6; down-modulated: p=0.33, t=1.1, N=6; Figs. 4M–N). These results are consistent with the ACC's known role in encoding novelty and prediction error.

For late tones (Fig. 4O), we observed a significant increase in EAPA peak amplitude during acquisition compared to pre-exposure (paired t-test, p=0.0053, t=4.7, N=6; Fig. 4P), with a trend toward increased AUC (p=0.055; t=2.5, N=6; Fig. 4Q). There were no differences in the proportions of modulated neurons (X^2=3.9, p=0.14; Figs. 4R–S), and mean response amplitudes among modulated neurons were not significantly different (up: p=0.1678, t=1.682, Fig. 4T; down: p=0.6859, t=0.4459, Fig. 4U).

These results provide evidence that, similar to the novelty of the US, the ACC encodes novelty of the CS during early tone exposures and has an enhanced response to the CS following repeated CS–US pairings.

Increased ACC modulation in response to CS cues following consolidation.

To specifically test the impact of offline consolidation on ACC activity after acquisition, we compared the activity of LR cell sets (n=1378 from 7 subjects) during early acquisition tones to the activity during the first five tones of the 24-h memory session. Fig. 5A shows the raster plot of events detected in a representative subject. The first five tones of both the 24-h and 48-h memory sessions were termed "recall" tones (fear recall and extinction recall, respectively), and the last five tones from these sessions were termed "extinction" tones. The early acquisition tones served as a baseline for pre-consolidation CS processing, representing recall of a benign cue; while the 24-h recall tones reflected post-consolidation memory retrieval. Within-session modulation of ACC activity is shown in Figure S5.

Although there was no significant difference in EAPA peak amplitude between acquisition and recall (p=0.14, t=1.7, N = 7; Fig. 5C), the overall response magnitude (AUC) was significantly greater during the recall tones compared to early acquisition (p=0.028, t=2.9, N = 7; Fig. 5D). This increase was accompanied by a substantial rise in the proportions of both up-modulated and down-modulated neurons (X^2=78, p<0.00001; Figs. 5E–F). The mean activity amplitude of both modulated subpopulations remained unchanged across sessions (Up-modulated: p=0.094, t=2.0, N=6; Down-modulated: p=0.21, t=1.4, N=6; Fig. 5G-H). These results show that the neuronal response to the CS in the ACC changed between early acquisition and recall, specifically showing a broader recruitment of neurons and enhanced EAPA, without changing the average firing rates of individual modulated neurons.

To determine whether there was overlap between subpopulations of neurons responsive to the CS and US between sessions, the number of neurons responsive to the CS and US during early acquisition, late acquisition, and recall were compared for expected vs. observed overlap (see Figures S3E, S4I and S5I). Neurons responsive to the CS or the US separately over time overlapped at a rate equivalent to chance (p>.05, X^2<4.8), suggesting no consistent subpopulations encoding the CS or US across presentations. However, neurons responsive to the US overlapped with neurons responsive to the CS at a rate lower than chance in both early (X^2=5.1, p=.024) and late (X^2=5.2, p=.023) acquisition. During 24-h recall, CS-responsive neurons and US-responsive neurons returned to overlapping at a rate equivalent to chance (p>.05, X^2<4.8). This pattern of results suggests that while there was a high degree of representational drift over time among cells representing the CS and US, subpopulations of CS-responsive and US-responsive neurons appeared to be distinct from each other during acquisition but indistinct following consolidation.

Decreased within-session modulation of the ACC in response to CS cues during extinction.

Next, we investigated whether ACC population activity showed any within-session adaptation following repeated exposure to the CS during the 24-h memory session. Comparison between the recall and extinction tones within the 24-h memory session showed that the CS elicited a progressively weakened response over time in all subjects (Fig. 5I). Although a within-session comparison of the kinetic parameters of the EAPA traces in response to the extinction tones showed no significant reduction in comparison to the recall tone responses (Amplitude: paired t-test, p=0.090, t=2.0, N=7; Figs. 5J, AUC: paired t-test, 0.43, t=0.85, N =7; Figs. 5K), the extinction tones modulated a smaller proportion of neurons than the recall tones in aggregate (X^2=95, p<0.00001; Figs. 5L-M). These results show that, with respect to the proportion of modulated neurons, the representation of the CS in the ACC during the 24-h memory session decreased from recall to extinction.

Subjects underwent a second fear extinction session (48-h memory) on the following day, consisting of an identical presentation of 15 tones. Within-session results

from the 48-h memory session closely mirrored those of the 24-h session (Figs. S6-S7), and there were no significant between-sessions differences in ACC response patterns (Fig. S8).

Evolution of ACC neuronal synchrony during acquisition, recall, and extinction of cued fear.

We next examined changes in neural synchrony both within and between the cue pre-exposure, acquisition, 24-h memory, and 48-h memory sessions, starting with the comparison of cue pre-exposure to acquisition (N=7 mice, N=1476 LR cell pairs; representative heatmaps are shown in Fig. 6A-D). We computed the maximum correlation and generated a cumulative distribution function (CDF) for each behavioral state. CDF curves were compared to each other and to the reference distribution ("Other"), representing unaligned neural activity within the same session. Both early and late tone presentations in each session resulted in an increase in neural synchrony relative to Other (cue pre-exposure: early, $p<0.0001$, $W=-4.7\times10^5$; late, $p<0.0001$, $W=-4.1\times10^5$; acquisition: early, $p<0.0001$, $W=-2.9\times10^5$; late, $p<0.0001$, $W=-3.3\times10^5$; Fig. 6E). The CDF curve for late cue pre-exposure was shifted leftward relative to early cue pre-exposure (Cohen's $d=-0.072$; $p=0.0049$) and relative to early acquisition (Wilcoxon signed rank: $p=0.0041$, $W=-9.4\times10^4$), indicating stronger correlations in response to early tones and a loss of synchrony over time. In contrast, the CDF curve for late acquisition was shifted to the right relative to early acquisition (Cohen's $d=0.060$; $p=0.020$), indicating stronger correlations in response to late tones and an increase in neural synchrony over time. The late tones presented during acquisition and pre-exposure sessions evoked comparable neural synchrony (Wilcoxon signed rank: $p=0.36$, $W = 3.1\times10^4$). Nonetheless, the effect sizes of all differences in neural synchrony in the cue pre-exposure and acquisition sessions were small.

To determine how the neural synchrony changed following offline consolidation, we compared the neural synchrony between early and late tones delivered during the acquisition and 24-h memory sessions (N=7 mice, N=1378 LR cell pairs; Figs. 6F-I). A large leftward shift, indicating a reduction in neural synchrony, was observed in the CFD plots for both the recall and extinction tones of the 24-h memory session relative to acquisition (recall: $p<0.0001$, $W=-3.3\times10^5$; extinction: $p<0.0001$, $W=-4.5\times10^5$; Fig. 6J), indicating a dramatic loss of neural synchrony following consolidation. This reduction in neural synchrony was also observed when comparing the reference distributions between sessions (Wilcoxon signed rank: Other (acquisition) vs. Other (24-h memory), $p<0.0001$, $W=-3.6\times10^5$). As before, neural synchrony in this LR cell set increased from early to late acquisition (Cohen's $d=0.097$; $p=0.0018$); while neural synchrony in the 24-h memory session dropped from recall to extinction (Cohen's $d=-0.069$, $p= 0.014$). Nonetheless, these within-session changes in CS-evoked neural synchrony were very small, particularly in comparison to the very large drop in ACC-wide neural synchrony following offline consolidation.

Finally, we compared the neural synchrony both within and between the 24-h and 48-h memory sessions (N=5 mice, N=1061 LR cell pairs). Neural synchrony in this LR cell set decreased from recall to extinction within both the 24-h memory and 48-h memory sessions (24-h: Cohen's d=-0.13, p=0.0001; 48-h memory: Cohen's d=-0.15, p=0.0001). Neural synchrony also decreased between the 24-h and 48-h memory sessions, both for recall tones and for extinction tones (recall: p=0.0053, W=-5.6×10^4; extinction: p=0.022, W=-4.6×10^4; Fig. S9E). There was no significant difference between the reference distributions for these two sessions (Other (24h) vs Other (48h): p=0.0601; W=3.8×10^4). Collectively, these results indicate that neural synchrony during the CS decreases from early to late cue pre-exposure, as novelty decreases; increases from early to late acquisition, as the CS becomes associated with the US; dramatically and globally decreases following offline consolidation; and continues to reduce over the course of extinction.

Discussion

We hypothesized that the ACC plays an active role in representing the negative valence of cues that predict adverse events. We observed a pattern of dynamic changes in the response of the ACC to a conditioned stimulus over the course of fear acquisition, recall, and extinction that was consistent with this hypothesis. The proportion of neurons modulated by the CS rose during acquisition, peaked during recall, and fell during extinction. At the same time, there were complementary changes in the population activity traces, but no changes in the relative activity of modulated subpopulations, suggesting that the primary contributor to changes in population activity was the recruitment of responsive neurons. This pattern of responses suggests dynamic changes in neural responses in the ACC concurrent with dynamic changes in the valence of the CS over the stages of the fear conditioning paradigm. As expected, we also saw evidence of the canonical roles of the ACC in responding to a painful US and in encoding the novelty of both the CS and US. Importantly, the responses of specific longitudinally registered cells in the ACC to the CS and the US over time showed no evidence of overlap and a high degree of representational drift, suggesting that the responses were not encoded by consistent subpopulations of cells or "engrams." Instead, novelty and valence of the CS were consistently encoded by changes in the dynamic recruitment of cortical neurons.

The fear conditioning paradigm serves as the cornerstone for studying the learned association between cues and threatening events (23-26). Behaviorally, our subjects successfully formed a learned association between the CS and US, as evidenced by increased freezing to the last two tones in the acquisition session and to the recall tones of the 24-h memory session. Our subjects showed high fear retention and failed to extinguish their learned fear responses following two 15-tone extinction sessions. This lack of behavioral extinction may have been due to an insufficient number of extinction tones, or could have resulted from maintaining an unchanged

context from acquisition to extinction. Nonetheless, the response of the ACC did extinguish over the course of memory sessions, particularly with respect to the proportions of modulated neurons (Figs. 7A-B). This difference between behavioral responses and neuronal correlates in the ACC suggests that other brain regions are responsible for maintaining the freezing response.

In general, freezing states during a CS were accompanied by a higher percentage of down-modulated neurons and a greater degree of neural synchrony in the ACC in all the sessions. Neither freezing during neutral habituation nor freezing in a context recently associated with shocks were accompanied by changes in firing activity relative to movement, suggesting that the neural response in the ACC during freezing was specific to cued fear and not contextual fear or neutral immobility. Nonetheless, the onset of the CS or the onset of CS-evoked population activity did not consistently coincide with the onset of freezing behavior. Together, the results suggest that the freezing state corresponds to changes in modulation of the ACC, but these changes in ACC activity are unlikely to drive the immediate expression of freezing behavior, instead playing a role in broader network-level processes.

The ACC is a key center for nociception and aversion processing (27-30). As expected, the ACC was significantly modulated by the US in all subjects. The ACC is also known to encode novelty and surprise (2, 6, 31, 32). We observed ACC response patterns consistent with novelty encoding, including larger EAPA amplitudes, more modulated neurons, and greater neural synchrony in response to the initial presentations of both the CS and the US. In contrast, another study showed that the magnitude of the responses of the neighboring prelimbic cortex to uncued foot shocks did not change over repeated presentations (20). These results suggest that the novelty of both neutral and aversive stimuli is encoded in the ACC by changes in the EAPA and in the proportion of modulated neurons.

Early reports using cued fear conditioning paradigms showed greater activation of the ACC when there was a delay between the end of the CS and onset of US (“trace”) compared to when the US immediately followed the CS (“delay”) (13). Consequently, ACC neural dynamics in “delay” fear conditioning paradigms have remained underexplored (16). Our results presented here using a “delay” paradigm are consistent with these prior reports in that, when all events in each session are averaged together, CS events presented during pre-exposure had a similar overall impact on ACC activity compared to CS events presented during acquisition. However, segregating these tones as early and late events in pre-exposure and acquisition sessions revealed that this lack of an effect was due to the overlapping representation in the ACC of the novelty and valence of the CS. Both the novelty of the CS, and the negative valence of the CS, were represented in the ACC by more modulated neurons, a larger EAPA response, and an increase in neural synchrony. This is consistent with other reports indicating that associative learning increases neuronal synchrony (33). Thus, future

paradigms intended to measure the representation of valence in the ACC need to properly control for and differentiate the representation of novelty.

One key advantage of longitudinal registration is the ability to track whether the population of individual neurons that are modulated in response to a stimulus changes over time, a concept known as “representational drift”. Along the lines of several new studies in other cortical areas (20, 34, 35), we observed a high degree of representational drift over time with respect to both the CS and US. Individual LR cells modulated by individual CS or US events during acquisition and recall overlapped with cells representing other events in the time series at rates consistent with chance. This high degree of representational drift suggests that the ACC employs a flexible and adaptive network during the encoding of fearful memories, rather than instantiating a static engram in which the same neurons are recruited across all phases of learning and memory. Interestingly, rather than overlapping, neurons representing the CS and US during acquisition were significantly distinct, suggesting that distinct subpopulations represent these stimuli prior to consolidation. Following consolidation, these populations became indistinct, overlapping by chance.

We propose that our results are most consistent with a role for the ACC in threat appraisal and a dynamic updating of short-term fear memories with the changing valence of a predictive cue. Fear memories are thought to be initially stored in the hippocampus and basolateral amygdala in stable engrams; over time, these memory traces are represented in neocortical regions, including the ACC, for long-term storage and remote recall (15, 36-39). Previous research has implicated the ACC and its projections to the hippocampus and amygdala in cued fear acquisition (10, 17), fear extinction (40), and short-term contextual fear recall (11, 19, 41), but some studies have suggested no role for the ACC in short-term cued fear recall (12, 18). Data presented here in our cued fear conditioning protocol show that CS-evoked EAPA responses and the proportion of CS-modulated neurons rose during acquisition, peaked following offline consolidation (during 24-h recall), and declined over the course of extinction, mirroring dynamic changes in the valence of the CS. Nonetheless, neurons modulated by the CS showed a high degree of representational drift, suggesting that CS responses were not driven by consistent, stable engrams. Event-associated population activity also failed to align temporally with the onset of freezing behavior, suggesting that neural responses were not directly driving freezing responses. A role for the ACC in dynamic updating of cued fear memories would explain both its necessity for fear learning processes, such as acquisition and extinction, and the lack of a causal role in short-term cued fear recall.

The findings in this study should be considered in light of its limitations. First and foremost, as a fully within-subjects study, this study is incapable of establishing cause-effect relationships among the observed effects. While we have shown a pattern of responses in the ACC consistent with the dynamic encoding of valence, we have not manipulated those responses to demonstrate that they affect behavioral outcomes,

although prior literature supports that conclusion (10, 17). Because all female subjects were eliminated from our cohort, our study includes only male subjects, and may not fully describe these same representations in females. We did not manipulate the context in our design, so the memory sessions represent overlapping contextual and cued fear responses. Our “early” and “late” time points during cue pre-exposure and acquisition contained only two tones each, increasing the random variability in responses. Finally, we did not observe behavioral fear extinction in our study, possibly due to insufficient extinction tones or the consistent context; therefore, our findings may represent an incomplete understanding of the representation of extinction in the ACC. Future studies seeking to follow up on these results might consider using more pre-exposure tones, more acquisition tones, and additional extinction sessions, along with a change of context from acquisition to recall/extinction.

In conclusion, this study highlights the dynamic and adaptive role of the ACC in detecting novelty, representing pain, and representing the valence of a conditioned cue as it changes dynamically across cued fear acquisition, consolidation, recall, and extinction. By dissociating the effects of novelty from associative learning, we revealed distinct patterns of ACC modulation that reflect its sensitivity to prediction error alongside its capacity for network plasticity. The observed representational drift and lack of direct correlation between ACC activity and onset of freezing behavior suggest that the ACC operates as a flexible integrative hub rather than a static repository for fear memories. While our findings align with theoretical models emphasizing the ACC’s canonical roles in encoding novelty, pain, and aversion, they also underscore its involvement in discriminating threatening cues from neutral cues during fear conditioning, and in continuously updating its representation of valence. Our findings are consistent with the interpretation that the ACC plays a role in threat appraisal and the representation of valence, and that it provides a learning signal that dynamically updates fear representations in other regions. These insights advance our understanding of the contributions of the ACC to fear memory processing and have implications for therapeutic strategies targeting dysregulated fear responses in anxiety and trauma-related disorders.

References

Acuña, M. A., Kasanetz, F., De Luna, P., Falkowska, M., & Nevian, T. (2023). Principles of nociceptive coding in the anterior cingulate cortex. *Proceedings of the National Academy of Sciences of the United States of America*, *120*(23), e2212394120. https://doi.org/10.1073/pnas.2212394120

Albo, Z., & Gräff, J. (2018). The mysteries of remote memory. *Philosophical Transactions of the Royal Society of London. Series B, Biological Sciences*, *373*(1742), 20170029. https://doi.org/10.1098/rstb.2017.0029

Alexander, W. H., & Brown, J. W. (2019). The Role of the Anterior Cingulate Cortex in Prediction Error and Signaling Surprise. *Topics in Cognitive Science*, *11*(1), 119–135. https://doi.org/10.1111/tops.12307

Bian, X.-L., Qin, C., Cai, C.-Y., Zhou, Y., Tao, Y., Lin, Y.-H., Wu, H.-Y., Chang, L., Luo, C.-X., & Zhu, D.-Y. (2019). Anterior Cingulate Cortex to Ventral Hippocampus Circuit Mediates Contextual Fear Generalization. *The Journal of Neuroscience: The Official Journal of the Society for Neuroscience*, *39*(29), 5728–5739. https://doi.org/10.1523/JNEUROSCI.2739-18.2019

Bissière, S., Plachta, N., Hoyer, D., McAllister, K. H., Olpe, H.-R., Grace, A. A., & Cryan, J. F. (2008). The rostral anterior cingulate cortex modulates the efficiency of amygdala-dependent fear learning. *Biological Psychiatry*, *63*(9), 821–831. https://doi.org/10.1016/j.biopsych.2007.10.022

Buckinx, A., Van Schuerbeek, A., Bossuyt, J., Allaoui, W., Van Den Herrewegen, Y., Smolders, I., & De Bundel, D. (2021). Exploring Refinement Strategies for Single Housing of Male C57BL/6JRj Mice: Effect of Cage Divider on Stress-Related Behavior and Hypothalamic-Pituitary-Adrenal-Axis Activity. Frontiers in behavioral neuroscience, 15, 743959. https://doi.org/10.3389/fnbeh.2021.743959

Canal, C. E., Chang, Q., & Gold, P. E. (2007). Amnesia produced by altered release of neurotransmitters after intraamygdala injections of a protein synthesis inhibitor. *Proceedings of the National Academy of Sciences of the United States of America*, *104*(30), 12500–12505. https://doi.org/10.1073/pnas.0705195104

Chen, T.-W., Wardill, T. J., Sun, Y., Pulver, S. R., Renninger, S. L., Baohan, A., Schreiter, E. R., Kerr, R. A., Orger, M. B., Jayaraman, V., Looger, L. L., Svoboda, K., & Kim, D. S. (2013). Ultrasensitive fluorescent proteins for imaging neuronal activity. *Nature*, *499*(7458), 295–300. https://doi.org/10.1038/nature12354

de Lima, M. A. X., Baldo, M. V. C., Oliveira, F. A., & Canteras, N. S. (2022). The anterior cingulate cortex and its role in controlling contextual fear memory to predatory threats. *eLife*, *11*, e67007. https://doi.org/10.7554/eLife.67007

Einarsson, E. Ö., & Nader, K. (2012). Involvement of the anterior cingulate cortex in formation, consolidation, and reconsolidation of recent and remote contextual fear memory. *Learning & Memory (Cold Spring Harbor, N.Y.)*, *19*(10), 449–452. https://doi.org/10.1101/lm.027227.112

Fendt, M., & Fanselow, M. S. (1999). The neuroanatomical and neurochemical basis of conditioned fear. *Neuroscience and Biobehavioral Reviews*, *23*(5), 743–760. https://doi.org/10.1016/s0149-7634(99)00016-0

Feng, P., Feng, T., Chen, Z., & Lei, X. (2014). Memory consolidation of fear conditioning: Bi-stable amygdala connectivity with dorsal anterior cingulate and medial prefrontal cortex. *Social Cognitive and Affective Neuroscience*, *9*(11), 1730–1737. https://doi.org/10.1093/scan/nst170

Frankland, P. W., Bontempi, B., Talton, L. E., Kaczmarek, L., & Silva, A. J. (2004). The involvement of the anterior cingulate cortex in remote contextual fear memory. *Science (New York, N.Y.)*, *304*(5672), 881–883. https://doi.org/10.1126/science.1094804

Frankland, P. W., Ding, H.-K., Takahashi, E., Suzuki, A., Kida, S., & Silva, A. J. (2006). Stability of recent and remote contextual fear memory. *Learning & Memory (Cold Spring Harbor, N.Y.)*, *13*(4), 451–457. https://doi.org/10.1101/lm.183406

Gansel, K. S. (2022). Neural synchrony in cortical networks: mechanisms and implications for neural information processing and coding. *Front. Integr. Neurosci., Oct 3:16:900715.* https://doi.org 10.3389/fnint.2022.900715

Ghosh, K. K., Burns, L. D., Cocker, E. D., Nimmerjahn, A., Ziv, Y., Gamal, A. E., & Schnitzer, M. J. (2011). Miniaturized integration of a fluorescence microscope. *Nature Methods*, *8*(10), 871–878. https://doi.org/10.1038/nmeth.1694

Goshen, I., Brodsky, M., Prakash, R., Wallace, J., Gradinaru, V., Ramakrishnan, C., & Deisseroth, K. (2011). Dynamics of retrieval strategies for remote memories. *Cell*, *147*(3), 678–689. https://doi.org/10.1016/j.cell.2011.09.033

Han, C. J., O'Tuathaigh, C. M., van Trigt, L., Quinn, J. J., Fanselow, M. S., Mongeau, R., Koch, C., & Anderson, D. J. (2003). Trace but not delay fear conditioning requires attention and the anterior cingulate cortex. *Proceedings of the National Academy of Sciences of the United States of America*, *100*(22), 13087–13092. https://doi.org/10.1073/pnas.2132313100

Hayden, B. Y., Heilbronner, S. R., Pearson, J. M., & Platt, M. L. (2011). Surprise signals in anterior cingulate cortex: Neuronal encoding of unsigned reward prediction errors driving adjustment in behavior. *The Journal of Neuroscience: The Official Journal of the Society for Neuroscience*, *31*(11), 4178–4187. https://doi.org/10.1523/JNEUROSCI.4652-10.2011

Heilbronner, S. R., & Hayden, B. Y. (2016). Dorsal Anterior Cingulate Cortex: A Bottom-Up View. *Annual Review of Neuroscience*, *39*, 149–170. https://doi.org/10.1146/annurev-neuro-070815-013952

Jhang, J., Lee, H., Kang, M. S., Lee, H.-S., Park, H., & Han, J.-H. (2018). Anterior cingulate cortex and its input to the basolateral amygdala control innate fear response. *Nature Communications*, *9*(1), 2744. https://doi.org/10.1038/s41467-018-05090-y

Jimenez, J. C., Berry, J. E., Lim, S. C., Ong, S. K., Kheirbek, M. A., & Hen, R. (2020). Contextual fear memory retrieval by correlated ensembles of ventral CA1 neurons. *Nature Communications*, *11*(1), 3492. https://doi.org/10.1038/s41467-020-17270-w

Kim, J. J., & Jung, M. W. (2006). Neural circuits and mechanisms involved in Pavlovian fear conditioning: A critical review. *Neuroscience and Biobehavioral Reviews*, *30*(2), 188–202. https://doi.org/10.1016/j.neubiorev.2005.06.005

Kitamura, T., Ogawa, S. K., Roy, D. S., Okuyama, T., Morrissey, M. D., Smith, L. M., Redondo, R. L., & Tonegawa, S. (2017). Engrams and circuits crucial for systems consolidation of a memory. *Science (New York, N.Y.)*, *356*(6333), 73–78. https://doi.org/10.1126/science.aam6808

Li, X.-H., Shi, W., Chen, Q.-Y., Hao, S., Miao, H.-H., Miao, Z., Xu, F., Bi, G.-Q., & Zhuo, M. (2023). Activation of the glutamatergic cingulate cortical-cortical connection facilitates pain in adult mice. *Communications Biology*, *6*(1), 1247. https://doi.org/10.1038/s42003-023-05589-1

Marek, R., Strobel, C., Bredy, T. W., & Sah, P. (2013). The amygdala and medial prefrontal cortex: Partners in the fear circuit. *The Journal of Physiology*, *591*(10), 2381–2391. https://doi.org/10.1113/jphysiol.2012.248575

Maren, S. (2001). Neurobiology of Pavlovian fear conditioning. *Annual Review of Neuroscience*, *24*, 897–931. https://doi.org/10.1146/annurev.neuro.24.1.897

McClelland, J. L., McNaughton, B. L., & O'Reilly, R. C. (1995). Why there are complementary learning systems in the hippocampus and neocortex: Insights from the successes and failures of connectionist models of learning and memory. *Psychological Review*, *102*(3), 419–457. https://doi.org/10.1037/0033-295X.102.3.419

Nadel, L., Samsonovich, A., Ryan, L., & Moscovitch, M. (2000). Multiple trace theory of human memory: Computational, neuroimaging, and neuropsychological results. *Hippocampus*, *10*(4), 352–368. https://doi.org/10.1002/1098-1063(2000)10:4<352::AID-HIPO2>3.0.CO;2-D

Niikura, K., Furuya, M., Narita, M., Torigoe, K., Kobayashi, Y., Takemura, Y., Yamazaki, M., Horiuchi, H., Enomoto, T., Iseki, M., Kinoshita, H., Tomiyasu, S., Imai, S., Kuzumaki, N., Suzuki, T., & Narita, M. (2011). Enhancement of glutamatergic transmission in the cingulate cortex in response to mild noxious stimuli under a neuropathic pain-like state. *Synapse (New York, N.Y.)*, *65*(5), 424–432. https://doi.org/10.1002/syn.20859

Patel, S., Johnson, K., Adank, D., & Rosas-Vidal, L. E. (2022). Longitudinal monitoring of prefrontal cortical ensemble dynamics reveals new insights into stress habituation. *Neurobiology of Stress*, *20*, 100481. https://doi.org/10.1016/j.ynstr.2022.100481

Peng, J.-Y., & Li, B.-M. (2009). Protein synthesis is essential not only for consolidation but also for maintenance and post-retrieval reconsolidation of acrobatic motor skill in rats. *Molecular Brain*, *2*, 12. https://doi.org/10.1186/1756-6606-2-12

Pissiota, A., Frans, O., Michelgård, A., Appel, L., Långström, B., Flaten, M. A., & Fredrikson, M. (2003). Amygdala and anterior cingulate cortex activation during affective startle modulation: A PET study of fear. *The European Journal of Neuroscience*, *18*(5), 1325–1331. https://doi.org/10.1046/j.1460-9568.2003.02855.x

Rolls, E. T. (2013). The mechanisms for pattern completion and pattern separation in the hippocampus. *Frontiers in Systems Neuroscience*, *7*, 74. https://doi.org/10.3389/fnsys.2013.00074

Rolls, E. T. (2019). The cingulate cortex and limbic systems for emotion, action, and memory. *Brain Structure & Function*, *224*(9), 3001–3018. https://doi.org/10.1007/s00429-019-01945-2

Steenland, H. W., Li, X.-Y., & Zhuo, M. (2012). Predicting aversive events and terminating fear in the mouse anterior cingulate cortex during trace fear conditioning. *The Journal of Neuroscience: The Official Journal of the Society for Neuroscience*, *32*(3), 1082–1095. https://doi.org/10.1523/JNEUROSCI.5566-11.2012

Tang, J., Ko, S., Ding, H.-K., Qiu, C.-S., Calejesan, A. A., & Zhuo, M. (2005). Pavlovian fear memory induced by activation in the anterior cingulate cortex. *Molecular Pain*, *1*, 6. https://doi.org/10.1186/1744-8069-1-6

Toyoda, H., Li, X.-Y., Wu, L.-J., Zhao, M.-G., Descalzi, G., Chen, T., Koga, K., & Zhuo, M. (2011). Interplay of amygdala and cingulate plasticity in emotional fear. *Neural Plasticity*, *2011*, 813749. https://doi.org/10.1155/2011/813749

Vassena, E., Deraeve, J., & Alexander, W. H. (2020). Surprise, value and control in anterior cingulate cortex during speeded decision-making. *Nature Human Behaviour*, *4*(4), 412–422. https://doi.org/10.1038/s41562-019-0801-5

Wu, D., Deng, H., Xiao, X., Zuo, Y., Sun, J., & Wang, Z. (2017). Persistent Neuronal Activity in Anterior Cingulate Cortex Correlates with Sustained Attention in Rats Regardless of Sensory Modality. *Scientific Reports*, *7*(1), 43101. https://doi.org/10.1038/srep43101

Zhao, R., Zhou, H., Huang, L., Xie, Z., Wang, J., Gan, W.-B., & Yang, G. (2018). Neuropathic Pain Causes Pyramidal Neuronal Hyperactivity in the Anterior Cingulate Cortex. *Frontiers in Cellular Neuroscience*, *12*, 107. https://doi.org/10.3389/fncel.2018.00107

Zhou, P., Resendez, S. L., Rodriguez-Romaguera, J., Jimenez, J. C., Neufeld, S. Q., Giovannucci, A., Friedrich, J., Pnevmatikakis, E. A., Stuber, G. D., Hen, R., Kheirbek, M. A., Sabatini, B. L., Kass, R. E., & Paninski, L. (2018). Efficient and accurate extraction of in vivo calcium signals from microendoscopic video data. *eLife*, *7*, e28728. https://doi.org/10.7554/eLife.28728

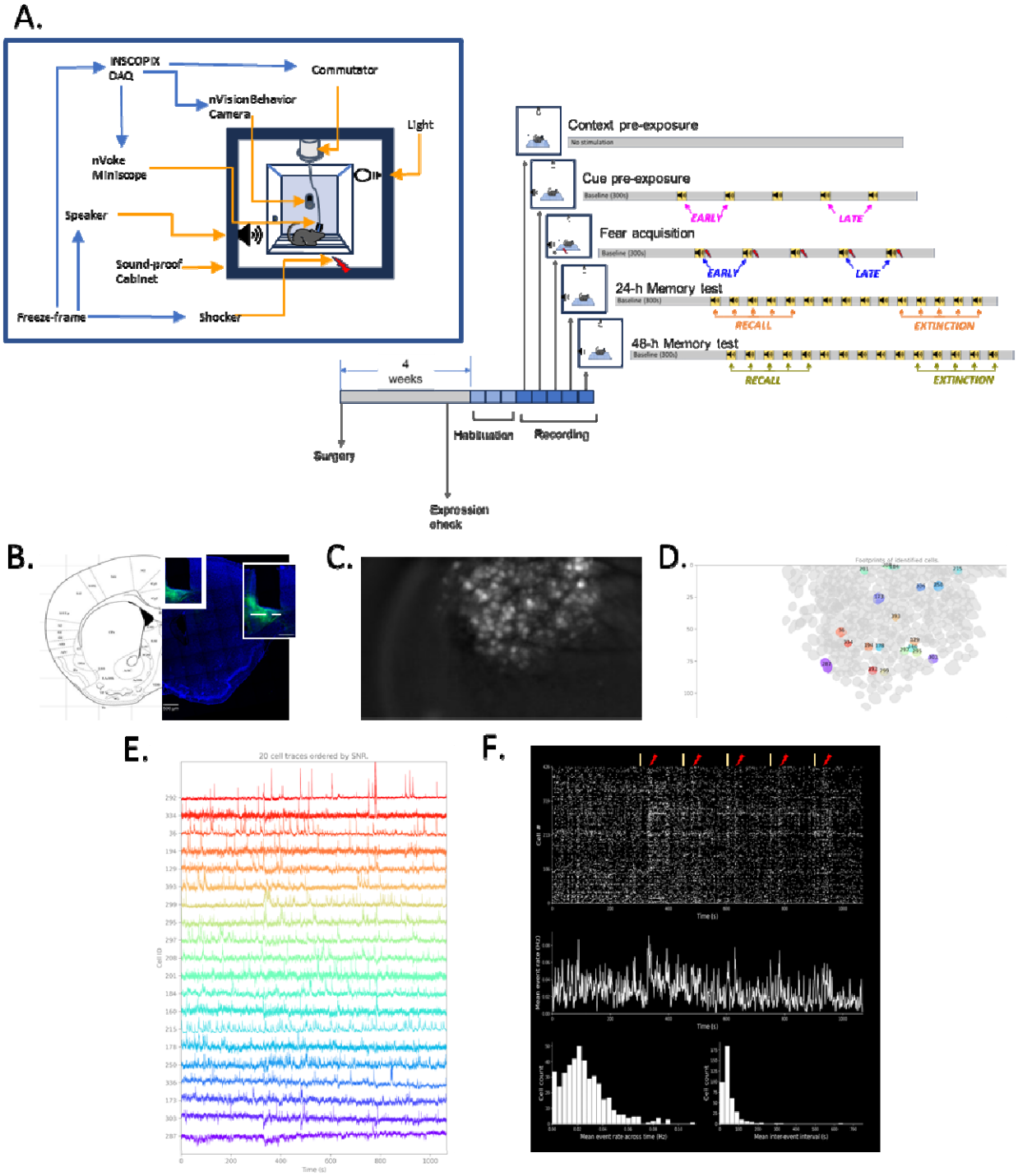

Figure 1: Experimental details of miniscope imaging in the mouse ACC.

A: Schematic illustration of the study timeline and behavioral paradigm. inset: Illustration showing the details of the experimental setup with blue arrows representing the TTL signals. **B:** Coronal atlas (left) and fluorescent image (right) showing the location of GCaMP6f expression and GRIN lens placement in the right ACC. Scale bar: 0.5 mm. Inset (white border) has been magnified to show GCaMP6f-expressing neurons

in the imaging plane (dashed line within inset; inset scale bar: 1 mm). **C:** Maximum projection of Ca^{2+} imaging movie file from all recorded neurons in a single session from the representative subject. **D:** Cell map generated from the maximum projection image from a representative animal showing the contours of the neurons extracted using the CNMFe algorithm. **E: F:** Raster plot of Ca^{2+} events during the acquisition session (day 3) of the experiment from the representative subject (top). The yellow and red marker lines represent the timing of the tone onset and foot shocks, respectively. The middle panel shows the change in the mean event rate of all the neurons over the time-course of a single recording session. The bottom panels show histograms depicting the frequency distribution of the mean event rate (left) and inter-event intervals (right) of the recorded Ca^{2+} events.

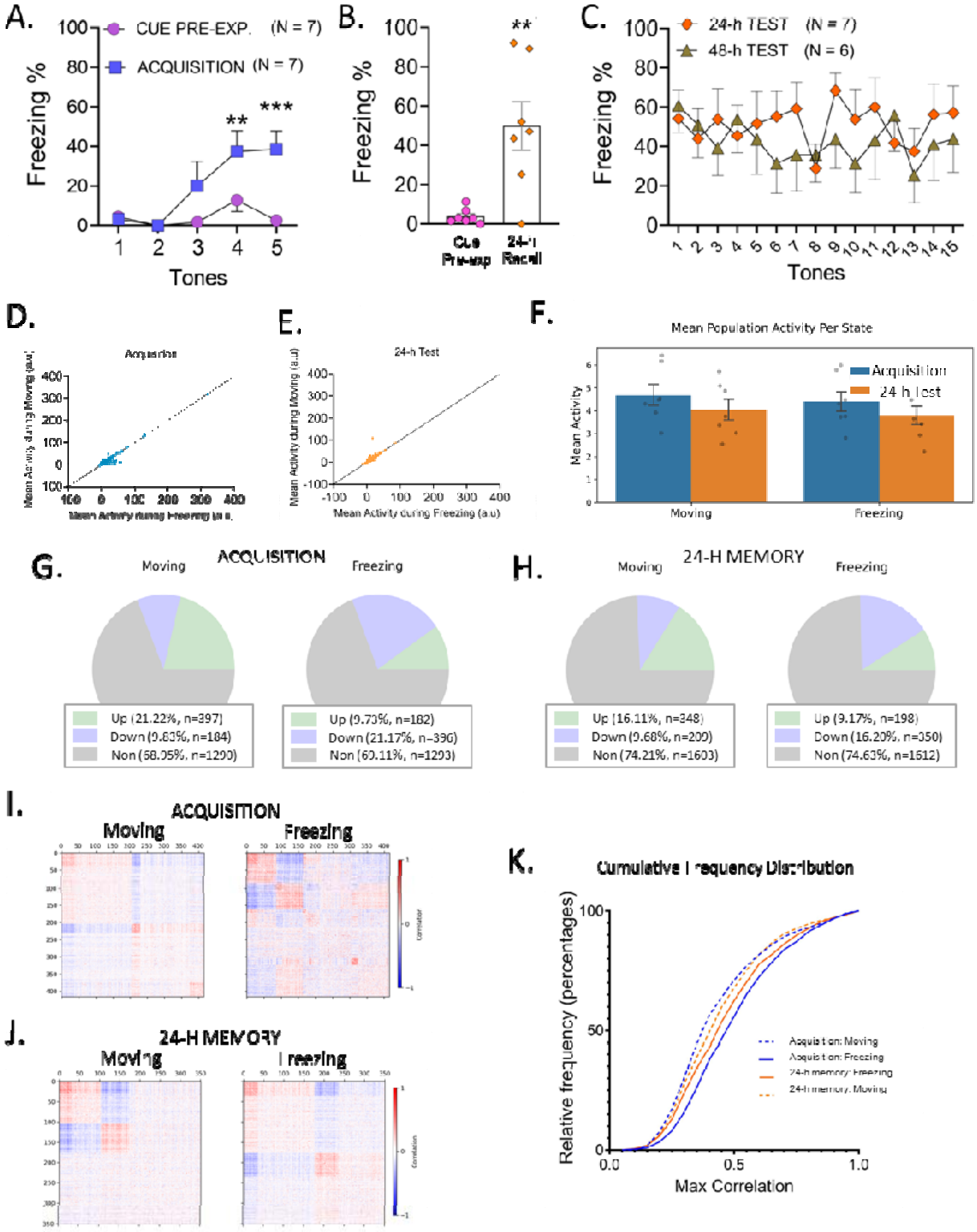

Figure. 2. Neural activity comparison during moving and freezing states across acquisition and memory sessions.

A: The change in freezing across tones during the cue pre-conditioning and acquisition sessions from N= 7 subjects. **B:** The mean freezing percentages in response to tones presented during cue pre-conditioning and the first five tones of the 24-h memory session (i.e. recall tones). **C:**. The change in freezing across tones during the 24-h and 48-h memory sessions. **D-E:** Scatter plots comparing mean neural activity during freezing versus moving during the acquisition (D) and 24-h memory (E) sessions. **F:** The average neural activity during moving and freezing states during the acquisition and the 24-h memory sessions. **G-H:** The proportion of neurons categorized by modulation group (Up-modulated, Down-modulated, or Non-modulated) for moving and freezing states during the acquisition (G) and 24-h memory (H) sessions. **I-J:** Heatmaps representing pairwise Pearson correlations between neurons during moving and freezing states in the acquisition (I) and 24-h memory (J) sessions. The color scale indicates the strength of correlation (red: high correlation, blue: low correlation). **K:** Cumulative frequency distribution plot comparing the maximum correlation of neurons between moving and freezing states across the acquisition and 24-h memory sessions.

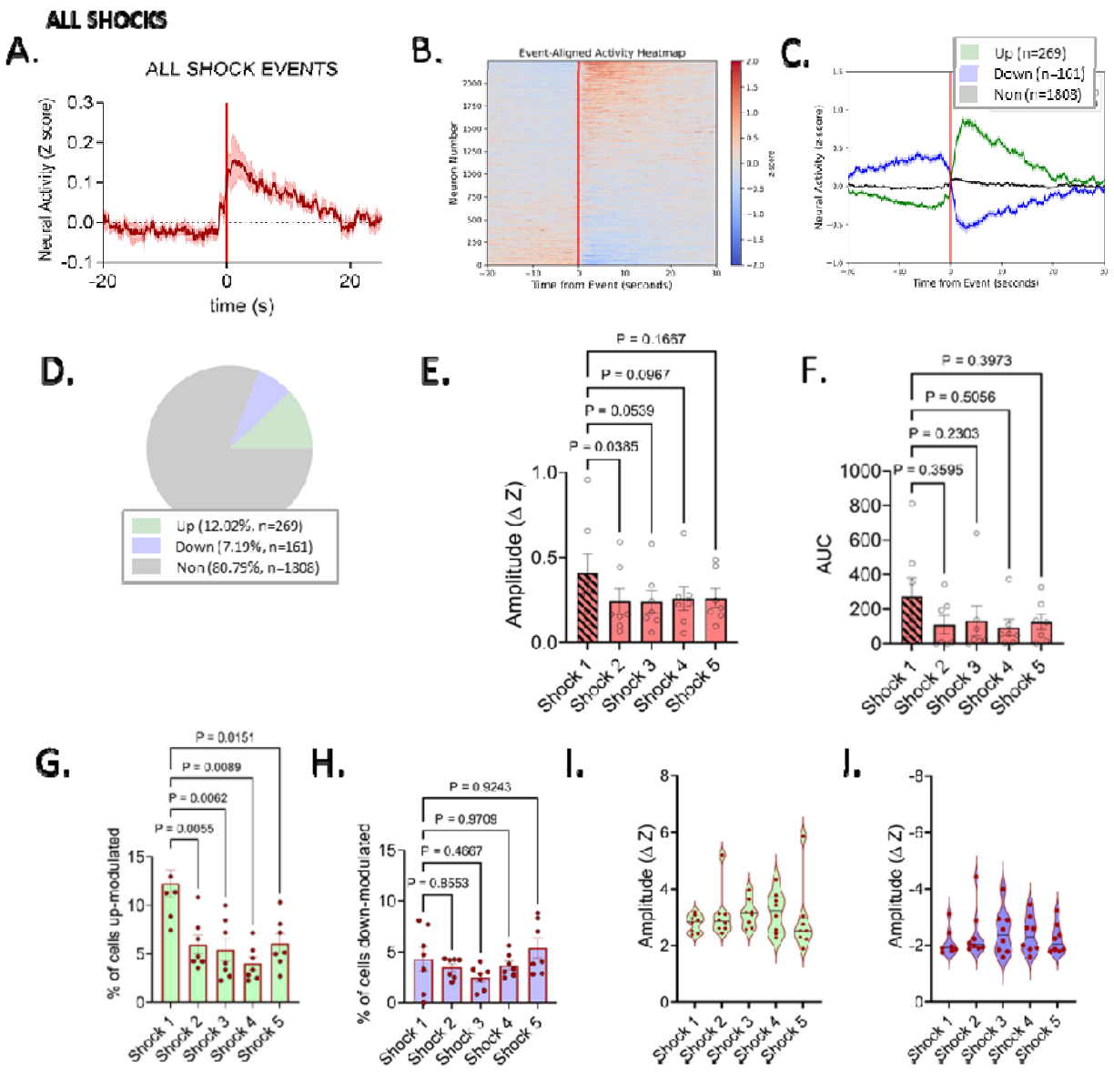

Figure 3: Neural activity during shock events across multiple shocks.
A: Mean event-associated population activity across all shock events. **B:** Heatmap of event-aligned neural activity across all shock events, with the red line marking the time of the shock. The color scale indicates the magnitude of neural response (red: high activity, blue: low activity). **C:** Comparison of neural activity during shock events between modulated subpopulations of neurons. **D:** The proportions of modulated neurons during shock events. **E-J:** Comparison between individual shock events. (E-F) Bar plot showing the change in the peak amplitude (E) and AUC (F) of neural responses across the first five shocks. (G-H) Percentage of neurons up-modulated (G) and down-modulated (H) across the five shocks. (I-J) The peak response amplitude across the five shocks for up-modulated (I) and down-modulated (J) neurons.

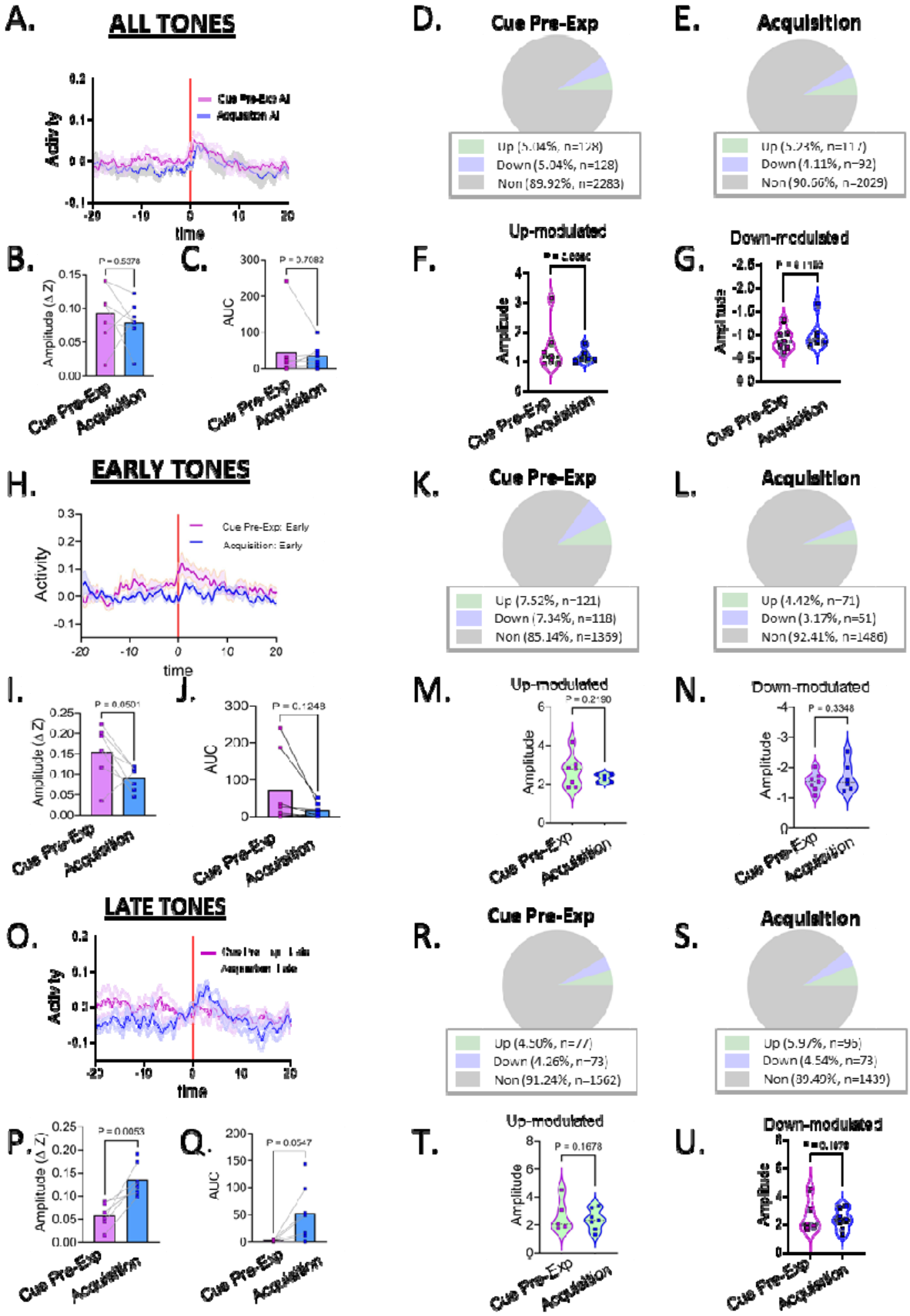
A.
ALL TONES
Activity
time
B.
Amplitude (Δ Z)
Cue Pre-Exp
Acquisition
C.
AUC
D.
Cue Pre-Exp
Up (5.04%, n=128)
Down (5.04%, n=128)
Non (89.92%, n=2283)
E.
Acquisition
Down (4.11%, n=92)
Non (90.56%, n=2029)
F.
Up-modulated
Amplitude
G.
Down-modulated
H.
EARLY TONES
Cue Pre-Exp: Early
Acquisition: Early
I.
J.
K.
Up (7.52%, n=121)
Down (7.34%, n=118)
Non (85.14%, n=1369)
L.
Up (4.42%, n=71)
Down (3.17%, n=51)
Non (92.41%, n=1486)
M.
N.
O.
LATE TONES
P.
Q.
R.
Up (4.50%, n=77)
Down (4.26%, n=73)
Non (91.24%, n=1562)
S.
Down (4.54%, n=73)
T.
U.

Figure 4: Neural activity comparison across tone events between the cue pre-exposure and acquisition sessions.

A-G: Comparison between all tones in the cue pre-exposure and acquisition sessions. (A) Event-associated population activity traces among longitudinally recorded neurons in response to all tones delivered in the cue pre-exposure and acquisition sessions. (B-C) Bar plots comparing amplitude (B) and AUC (C) for all tones across the two conditions. (D-E) Pie charts representing the proportions of modulated neurons for all tones during cue pre-exposure (D) and acquisition (E) sessions. (F-G) Violin plots comparing the amplitude of the change in activity of the up-modulated (F) and down-modulated (G) subpopulations of ACC neurons in response to all tones. **H-N:** Comparison between the early tones of the cue pre-exposure and acquisition sessions. (H) Event-associated population activity traces in response to the early tones delivered during the cue pre-exposure and acquisition sessions. (I-J) Bar plots comparing amplitude (I) and AUC (J) for the early tones between the two sessions. (K-L) Pie charts showing the change in the proportions of modulated neurons in response to the early tones during the cue pre-exposure (K) and acquisition (L) sessions. (M-N) Violin plots comparing the amplitude of the change in activity of the up-modulated (M) and down-modulated (N) subpopulations of ACC neurons in response to the early tones. **O-U:** Comparison between the <u>late</u> tones of the cue pre-exposure and acquisition sessions. O: Event-associated population activity traces in response to the late tones delivered during the cue pre-exposure and acquisition sessions. (P-Q) Bar plots comparing amplitude (P) and AUC (Q) for the late tones between the two sessions. (R-S) Pie Charts showing the change in the proportions of modulated neurons in response to the late tones during the cue pre-exposure (R) and acquisition (S) sessions. (T-U) Violin plots comparing the amplitude of the change in activity of the up-modulated (T) and down-modulated (U) subpopulations of ACC neurons in response to the late tones.

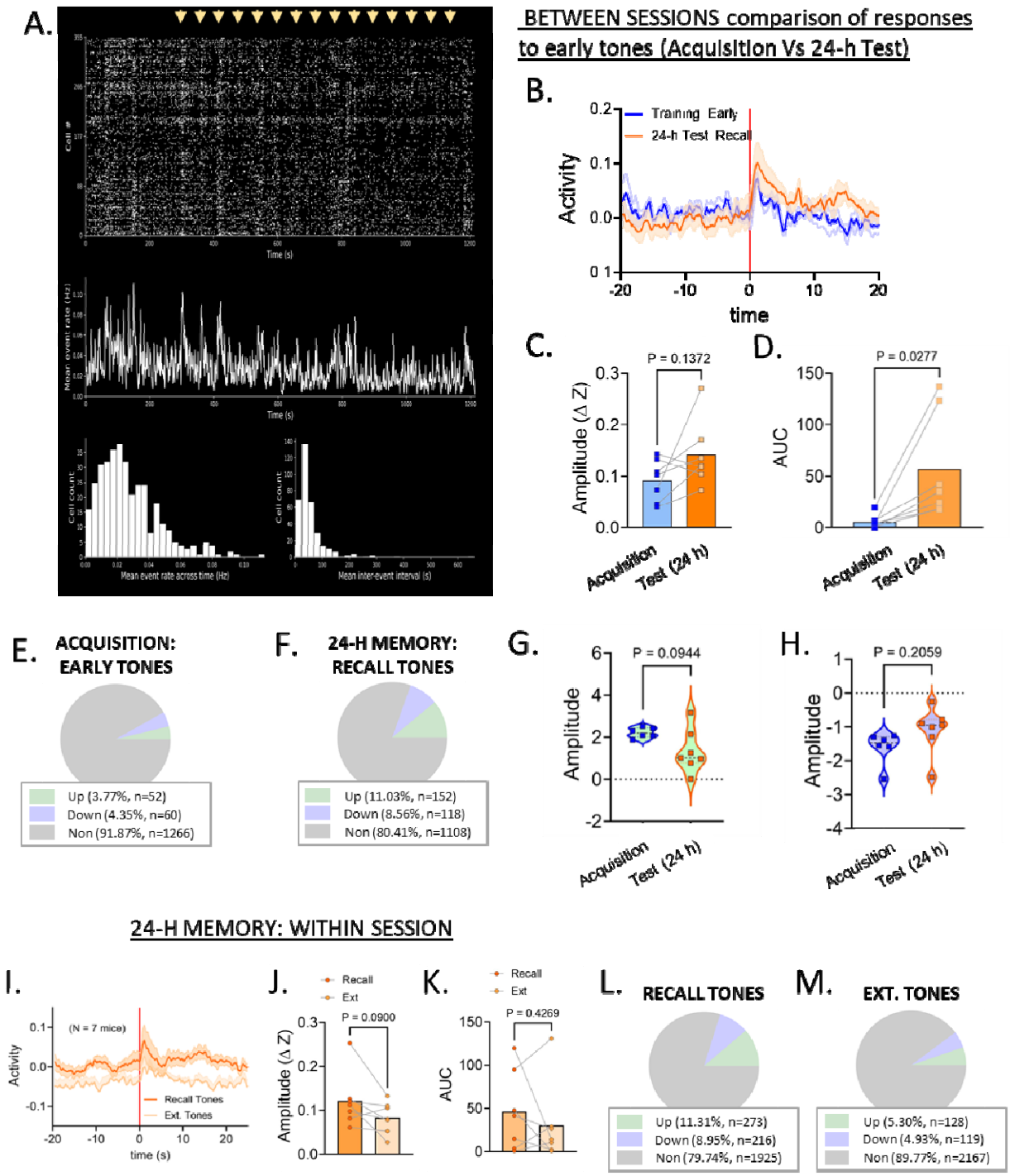

Figure 5: A: Top: Raster plot showing neural activity during the 24-h memory session. Yellow arrowheads represent CS presentations. Middle: Average neural activity trace across all recorded neurons from the representative subject. Bottom: Histograms representing the distribution of mean event rates and mean inter-event intervals. **B-H:** Between-sessions comparison of responses to early tones delivered during the acquisition and 24-h memory sessions. (B) Event-associated population activity traces

during early tones in the acquisition and 24-h memory sessions. (C-D) Bar plots comparing amplitude (C) and AUC (D) between early tones in the acquisition and 24-h memory sessions. (E-F) Pie charts showing the proportion of modulated neurons during early tones in the acquisition (E) and 24-h memory (F) sessions. (G-H) Violin plots comparing the amplitude of up-modulated neurons in early acquisition (G) and 24-h memory (H) sessions. **I-M:** Within-session analysis of ACC neural activity in response to recall and extinction tones during the 24-h memory session. (I) Event-associated population activity traces during recall and extinction tones in the 24-h memory session. (J-K) Bar plots comparing amplitude (J) and AUC (K) for recall and extinction tones during the 24-h memory session. (L-M) Pie charts showing the proportion of neurons modulated by recall tones (L) and extinction tones (M) during the 24-h memory session.

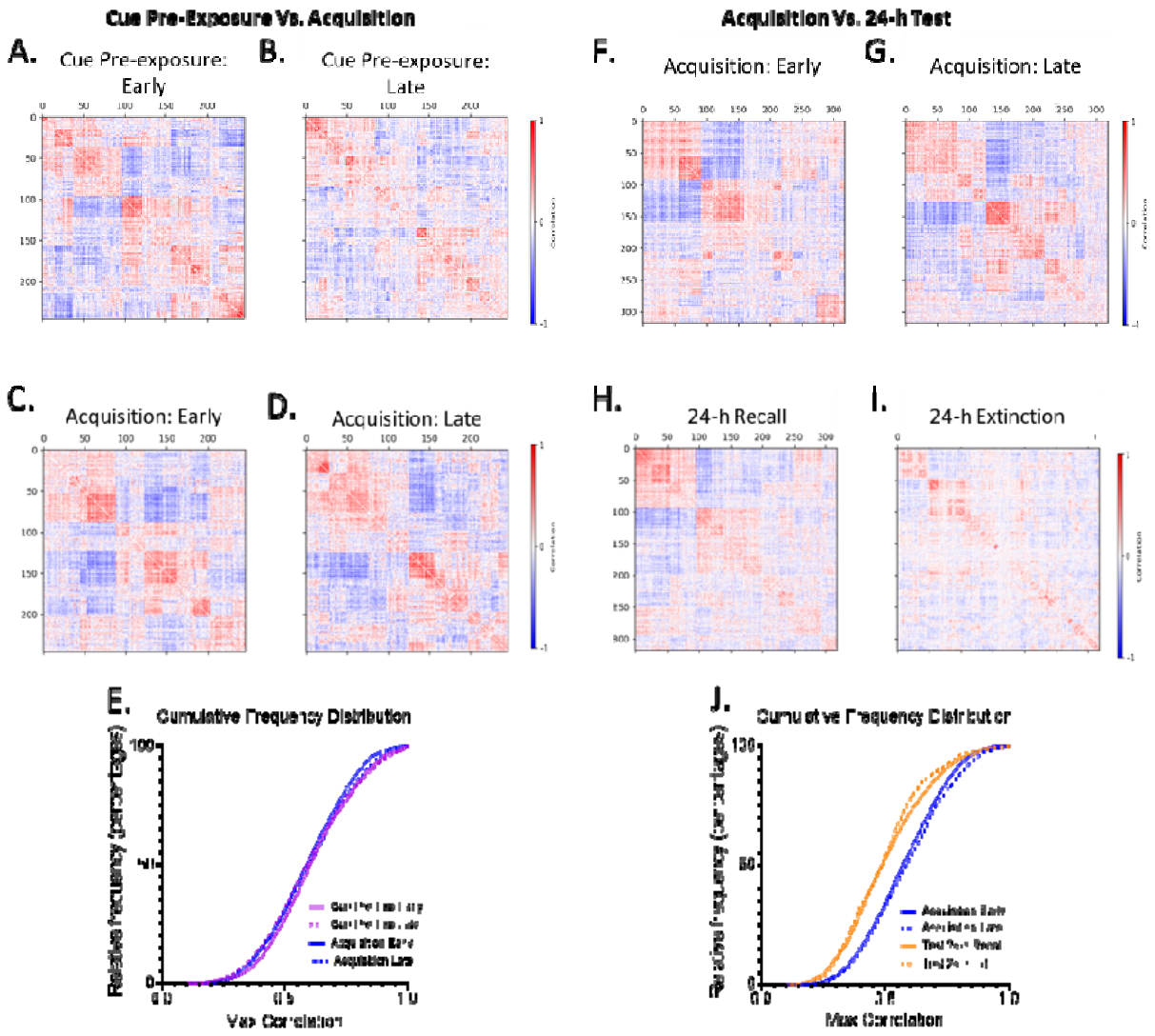

Figure 6: Correlation Analysis of Neural Activity Patterns Across Experimental Sessions. A-D: Heatmaps showing the correlations of neural activity response patterns between neurons within the (A) early cue pre-exposure, (B) late cue pre-exposure, (C) early acquisition, and (D) late acquisition tone presentations. Each pixel reflects the correlation coefficient between corresponding neural activity across sessions, with the color scale indicating correlation strength (red: high, blue: low). **E**: Cumulative frequency distribution of maximum correlations for early and late tones delivered in the cue pre-exposure and acquisition sessions. **F-I:**: Heatmaps showing the correlations of neural activity response patterns between neurons within the (F) early acquisition, (G) late acquisition, (H) early 24-h memory (recall), and (I) late 24-h memory (extinction) tone presentations. **J:** Cumulative frequency distribution of maximum correlations for early and late tones delivered in the acquisition and 24-h memory sessions.

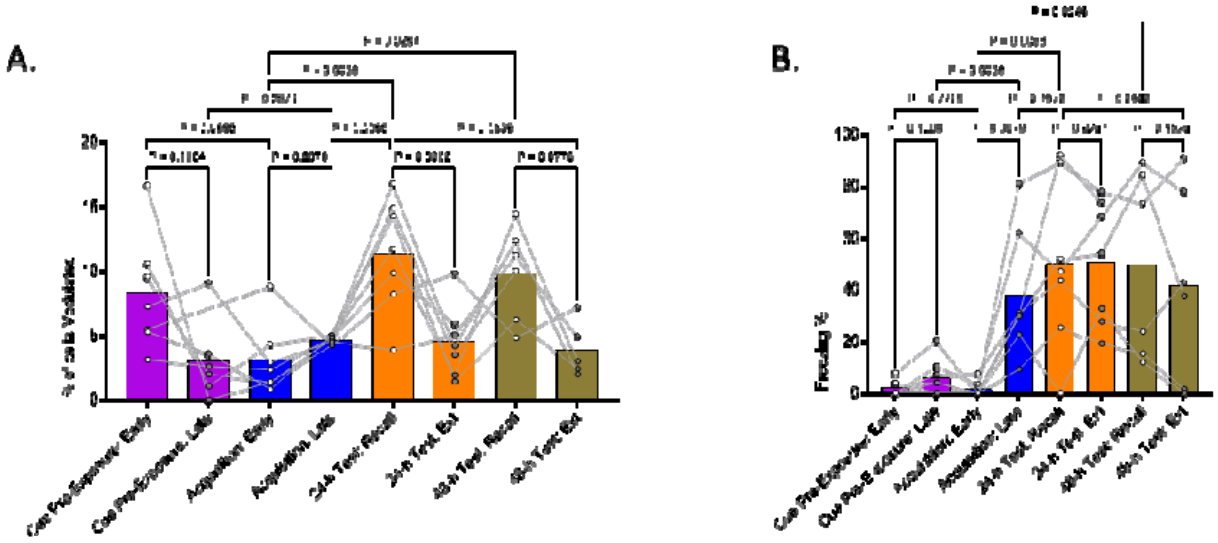

Figure 7: Summary comparison of ACC modulation and freezing behavior.

A: The percentage of ACC cells modulated (up and down combined) in response to the CS at different phases of the fear conditioning paradigm. **B:** The percentage of freezing displayed by the subjects in response to the CS in the same phases as in (A).

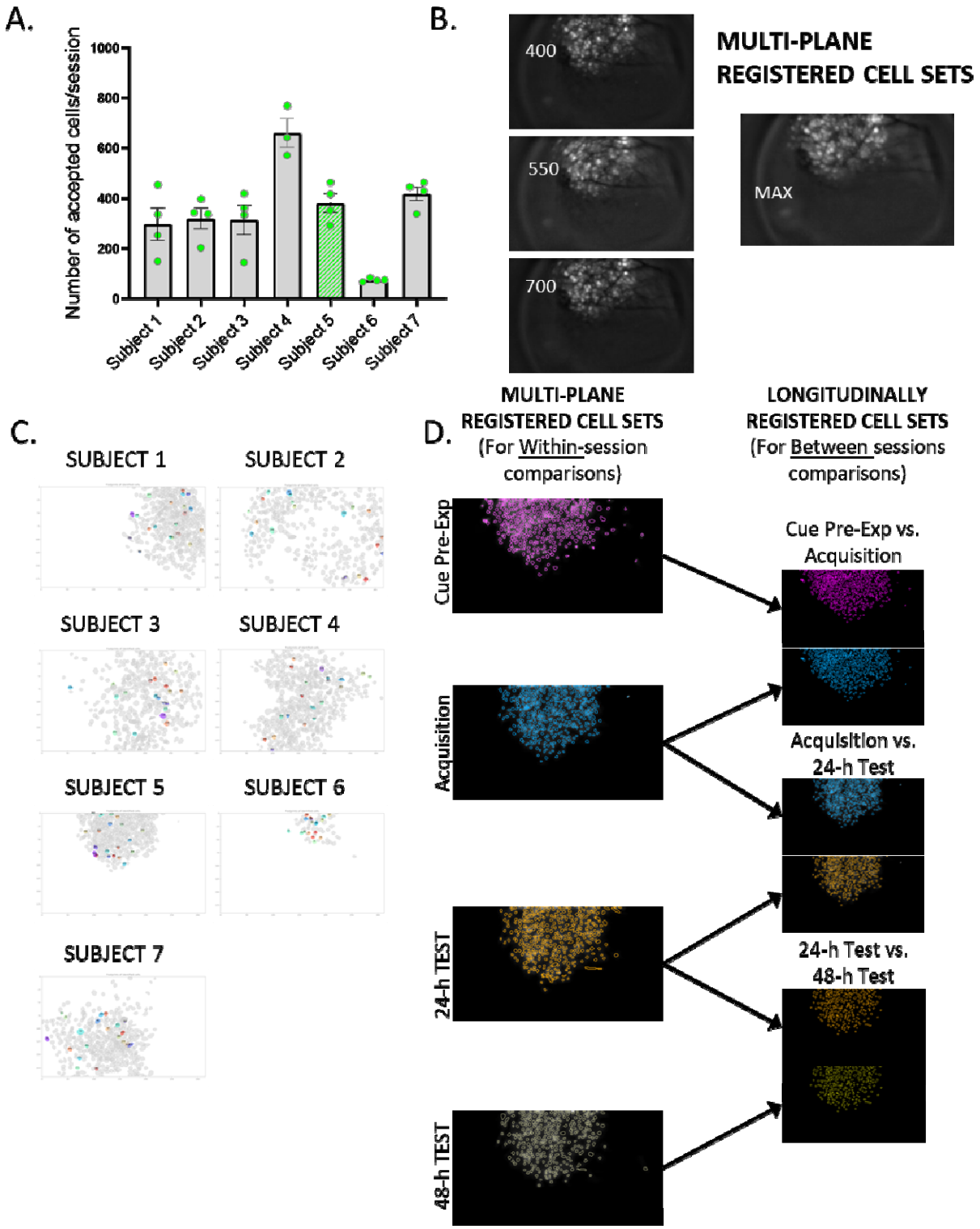

Supplementary Figure S1. Calcium imaging in mouse ACC.

A: Number of accepted neurons per session for each of the seven animals included in the study. The green-highlighted bar denotes the representative subject shown in the

main figures throughout the manuscript. **(B)** Multi-plane registration was performed across three focal planes (400, 550, and 700 units), allowing alignment of spatial footprints to generate a unified cell set per subject. The composite image (MAX) shows the merged cell map across planes. **(C)** Spatial footprints of accepted neurons during the cue pre-exposure session for each individual subject. **(D)** Schematic of the strategy for within- and between-session comparisons. Left column: all multi-plane registered neurons from individual sessions were included in within-session analyses. Right column: only longitudinally registered (LR) cells tracked across two successive sessions were used for between-session comparisons.

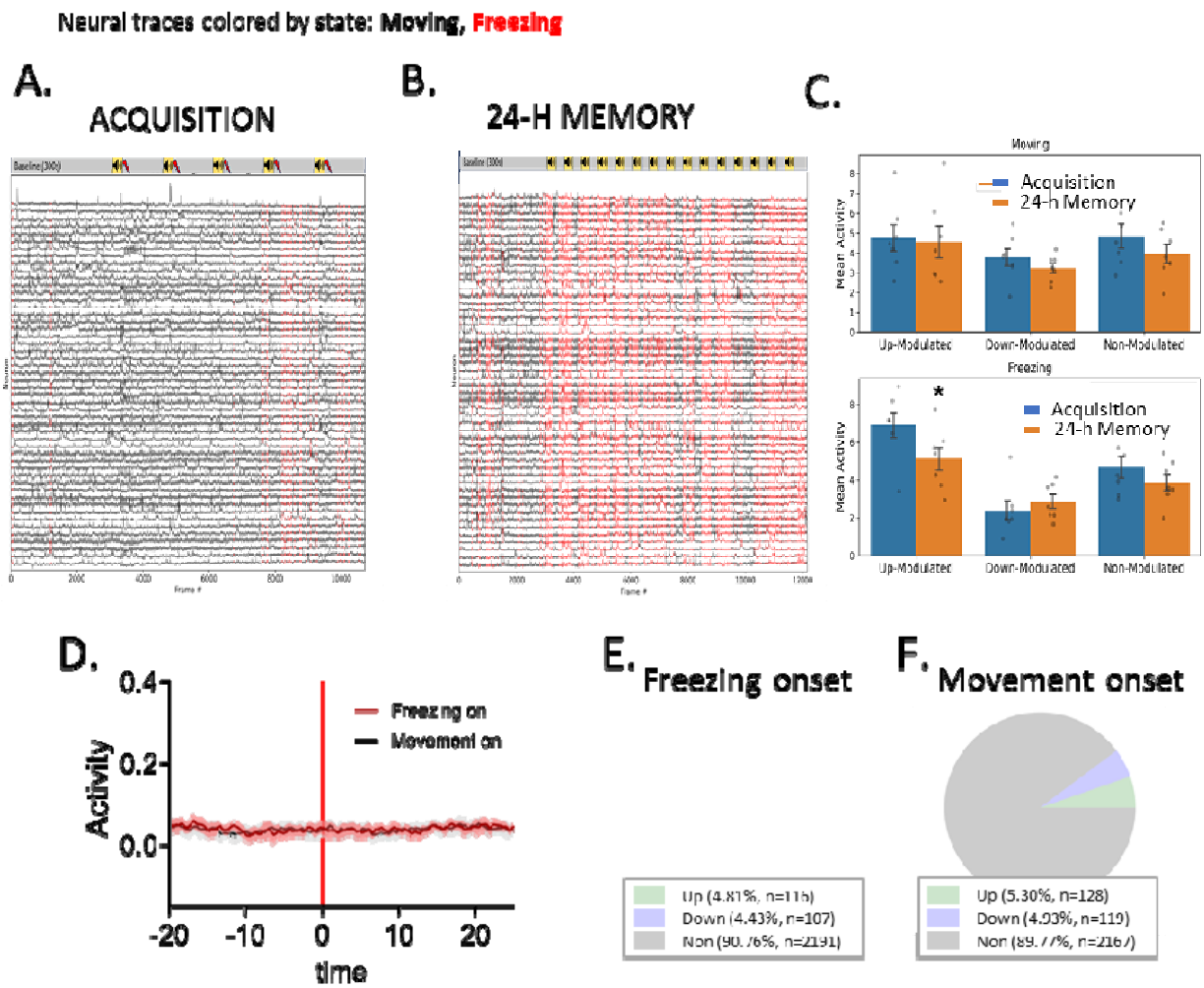

Supplementary Figure S2. Neural activity during moving and freezing states.

A-B. Raster plots showing neural activity traces during the acquisition (A) and 24-h memory (B) sessions, also color-coded by state (black = moving vs. red = freezing). **C.** The change in mean activity of ACC neurons per modulation group during the acquisition and 24-h memory sessions during moving (upper panel) and freezing (lower panel). The up-modulated fraction of neurons was significantly less active during freezing in the 24-h memory session (p=0.069, t=1.99). **D.** Event-aligned population activity of ACC neurons during moving and freezing in the first 300 s in the 24-h memory session. **E-F:** Pie charts comparing the fractions of up-, down- and non-modulated ACC neurons during the onset of moving (E) and freezing (F) in the first 300 s in the 24-h memory session.

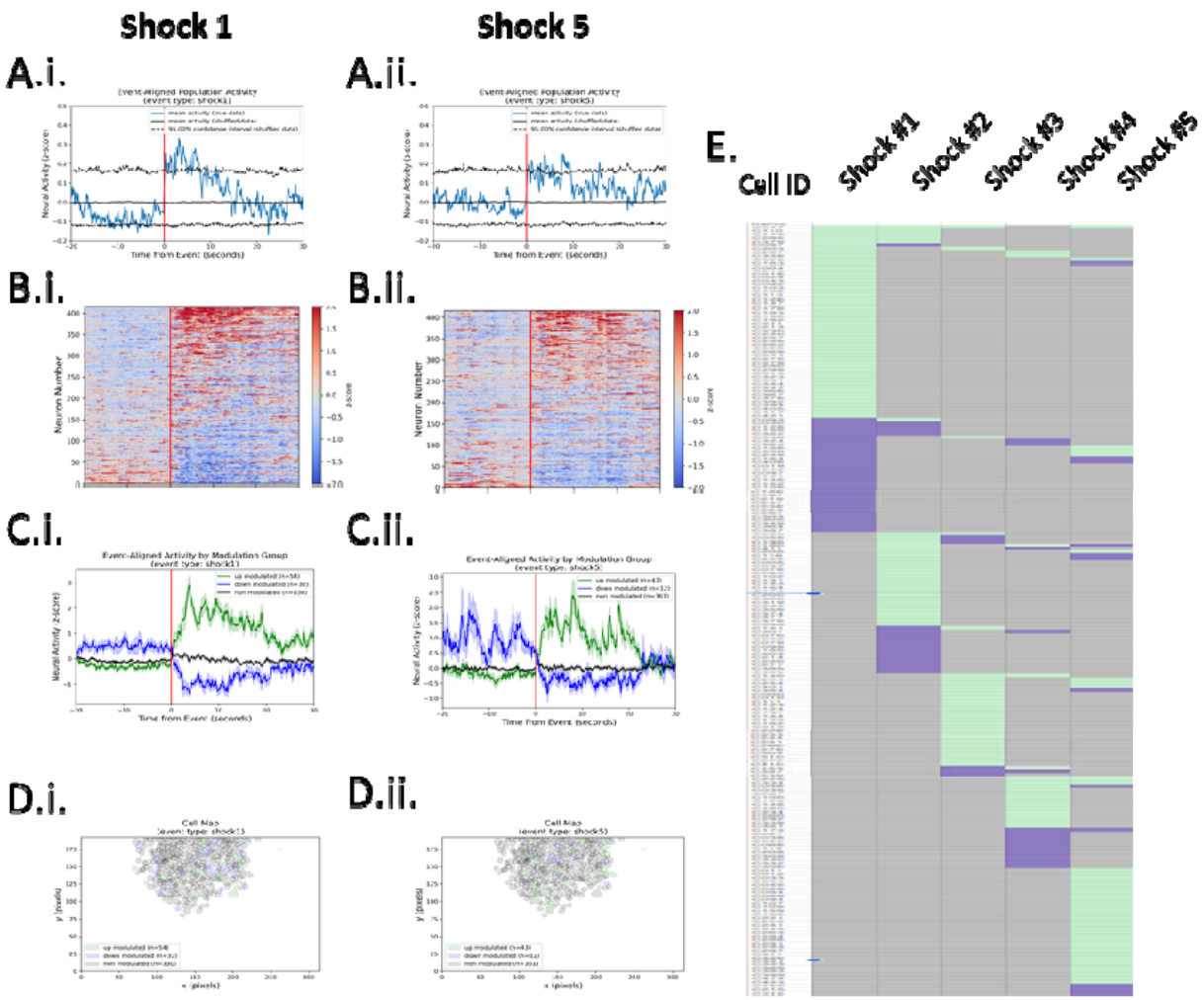

Supplementary Figure S3. Comparison of ACC neuron activity in response to the first and last US from a single subject. A.i-A.ii: Event-aligned population activity traces showing change of population activity over time in response to the first (A.i) and fifth foot shocks (A.ii) during the acquisition session. Red line represents timing of the delivery of the US events (t=0). **B.i-B.ii:** Heatmaps of event-aligned neural activity in response to the first (B.i) and fifth foot shocks (B.ii) during acquisition, each row representing individual neuron responses aligned to the time of the event. **C.i-C.ii:** Event-aligned activity traces for up-modulated (green), down-modulated (blue), and non-modulated (gray) neurons during the first (C.i) and fifth (C.ii) foot shocks. **D.i-D.ii:** Cell maps representing the spatial distribution of neurons modulated by the first (D.i) and fifth (D.ii) foot shocks. **E.** Heatmap showing individual neuron modulation states across all five US events within the same session. Each row represents a neuron and is color-coded based on modulation status, revealing how the responses of individual neurons change across US presentations in a single session.

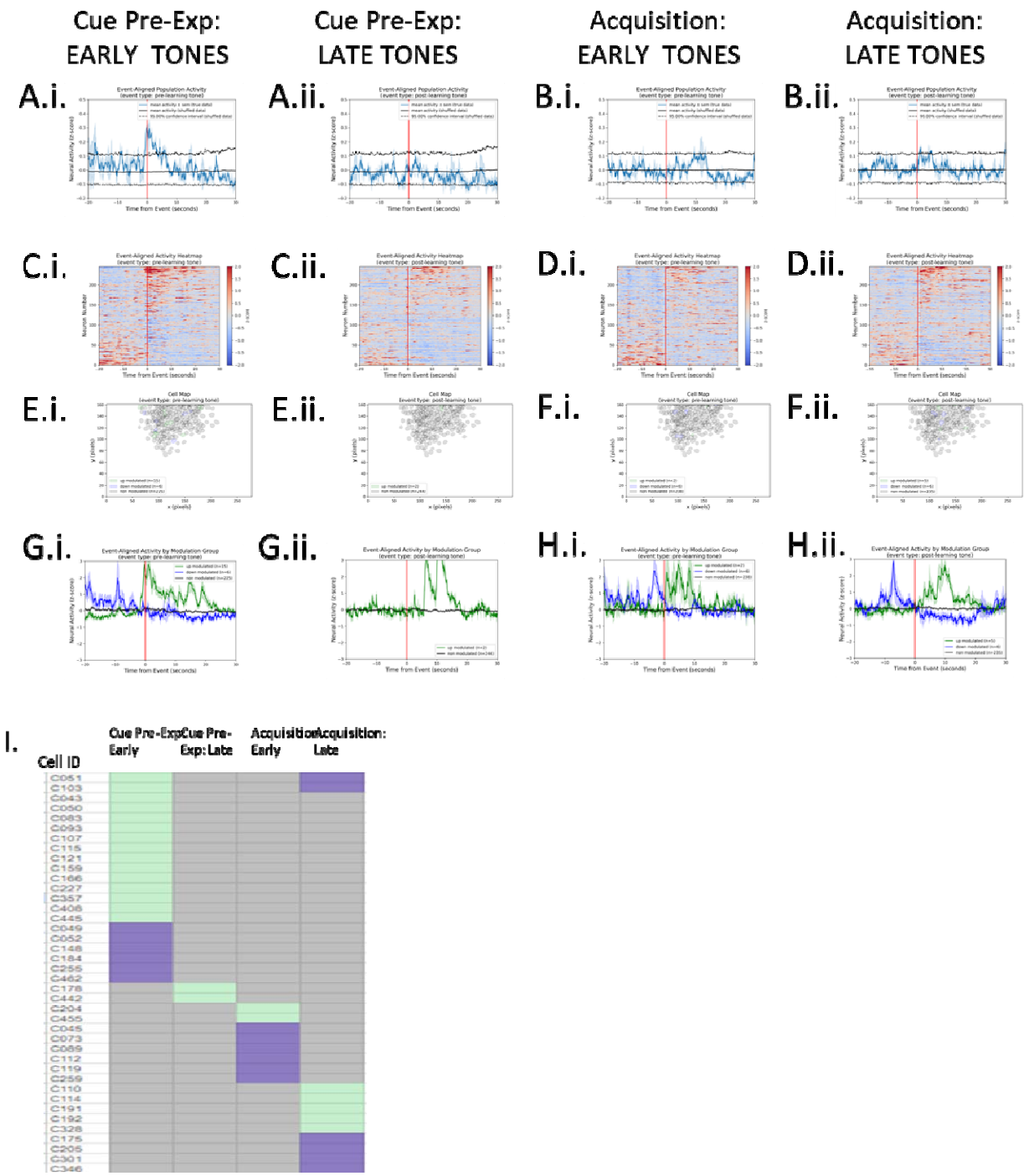

Supplementary Figure S4. Modulation of ACC activity in LR cell sets in response to early and late tones delivered during the cue pre-exposure and acquisition sessions from one representative subject.

A.i-A.ii: Event-aligned population activity traces showing change of population activity over time in response to early (A.i) and late tones (A.ii) during the cue pre-exposure session. **B.i-B.ii:** Event-aligned population activity traces showing change of population

activity over time in response to early (A.i) and late tones (A.ii) during the acquisition session. **C.i-C.ii:** Heatmaps of event-aligned neural activity for early (C.i) and late tones (C.ii) during cue pre-exposure session. **D.i-D.ii:** Heatmaps of event-aligned neural activity for early (D.i) and late tones (D.ii) during the acquisition session**. E.i-E.ii:** Cell maps representing the spatial distribution of neurons modulated by early tones (E.i) and late tones (E.ii) during the cue pre-exposure session. The neurons are color-coded based on modulation type (greeN=up-modulated, purple = down-modulated, or gray = non-modulated). **F.i-F.ii:** Cell maps representing the spatial distribution of neurons modulated by early tones (E.i) and late tones (E.ii) during acquisition. **G.i-G.ii:** Event-aligned activity traces for up-modulated (green), down-modulated (blue), and non-modulated (gray) neurons during early tones (G.i) and late tones (G.ii) in the cue pre-exposure session. **H.i-H.ii:** Event-aligned activity traces for modulated subpopulations of neurons during early (H.i) and late tones (H.ii) delivered during the acquisition session. **I:** Heatmap showing individual neuron modulation states across all conditions (cue pre-exposure: early, cue pre-exposure: late, acquisition: early, and acquisition: late). Each row represents a neuron, and each column represents a condition. Cells are color-coded based on modulation status, revealing how the responses of individual neurons change across the different tones and sessions.

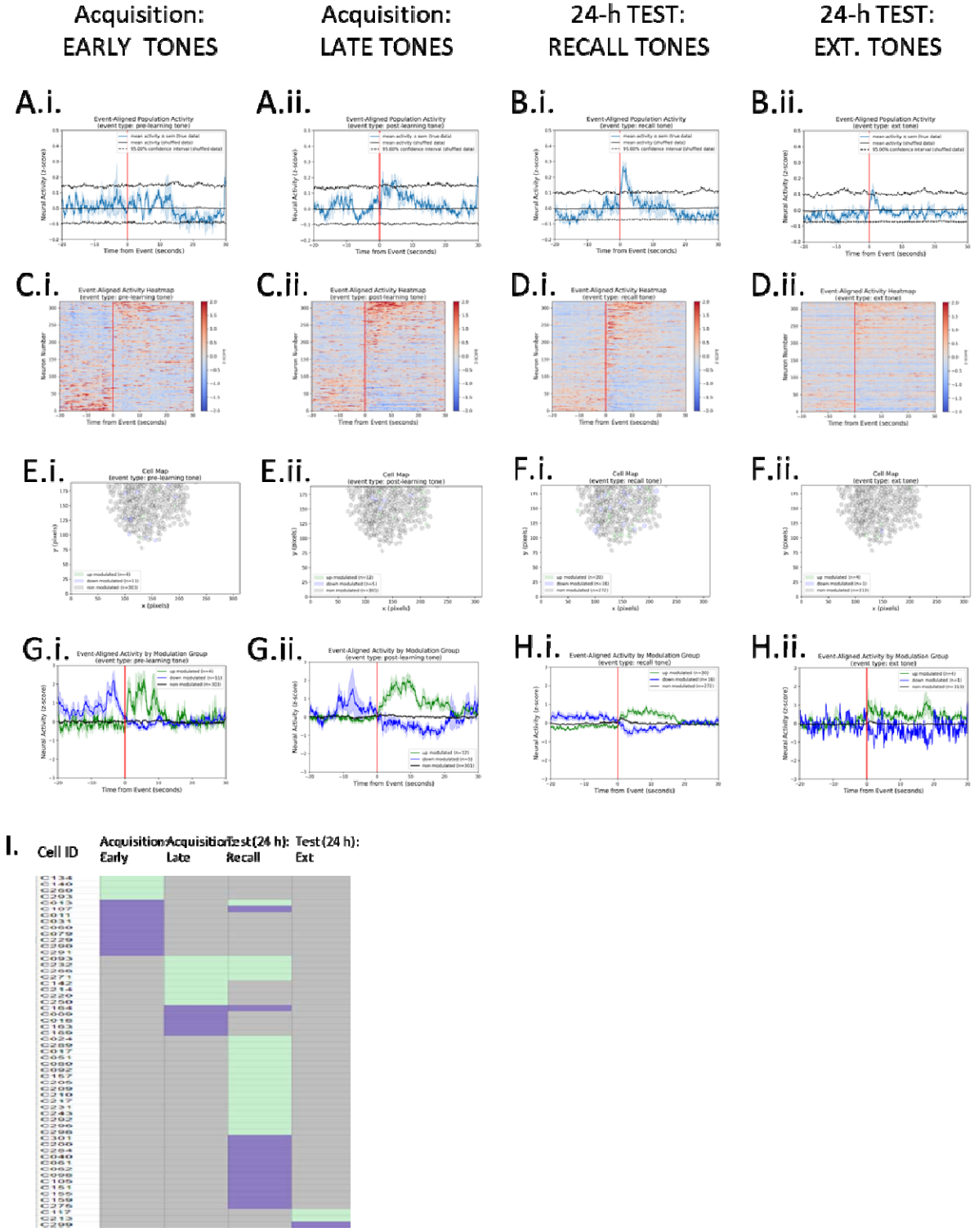

Supplementary Figure S5. Comparison of neural activity in response to CS during acquisition and memory sessions from one representative subject.

A.i-A.ii: Event-aligned population activity traces showing change of population activity over time in response to early (A.i) and late tones (A.ii) during the acquisition session.

B.i-B.ii: Event-aligned population activity traces for recall tones (B.i) and extinction tones (B.ii) during the 24-h memory session. **C.i-C.ii:** Heatmaps of event-aligned neural activity for early tones (C.i) and late tones (C.ii) during acquisition, each row representing individual neuron responses aligned to tone onset (red line). **D.i-D.ii:** Heatmaps of event-aligned neural activity for recall tones (D.i) and extinction tones (D.ii) during the 24-h memory session, showing the responses of individual neurons across time relative to tone onset. **E.i-E.ii:** Cell maps representing the spatial distribution of neurons modulated by early tones (E.i) and late tones (E.ii) during acquisition. The neurons are color-coded based on modulation type (greeN=up-modulated, purple = down-modulated, or gray = non-modulated). **F.i-F.ii:** Cell maps representing the distribution of neurons modulated by recall tones (F.i) and extinction tones (F.ii) during the 24-h memory session. **G.i-G.ii:** Event-aligned activity traces for up-modulated (green), down-modulated (blue), and non-modulated (gray) neurons during early tones (G.i) and late tones (G.ii) in the acquisition session. **H.i-H.ii:** Event-aligned activity traces for up-modulated, down-modulated, and non-modulated neurons during recall tones (H.i) and extinction tones (H.ii) in the 24-h memory session. **I:** Heatmap showing individual neuron modulation states across all conditions (acquisition early, acquisition late, 24-h recall, 24-h extinction). Each row represents a neuron, and each column represents a condition. Cells are color-coded based on modulation status, revealing how the responses of individual neurons change across the different tones and sessions.

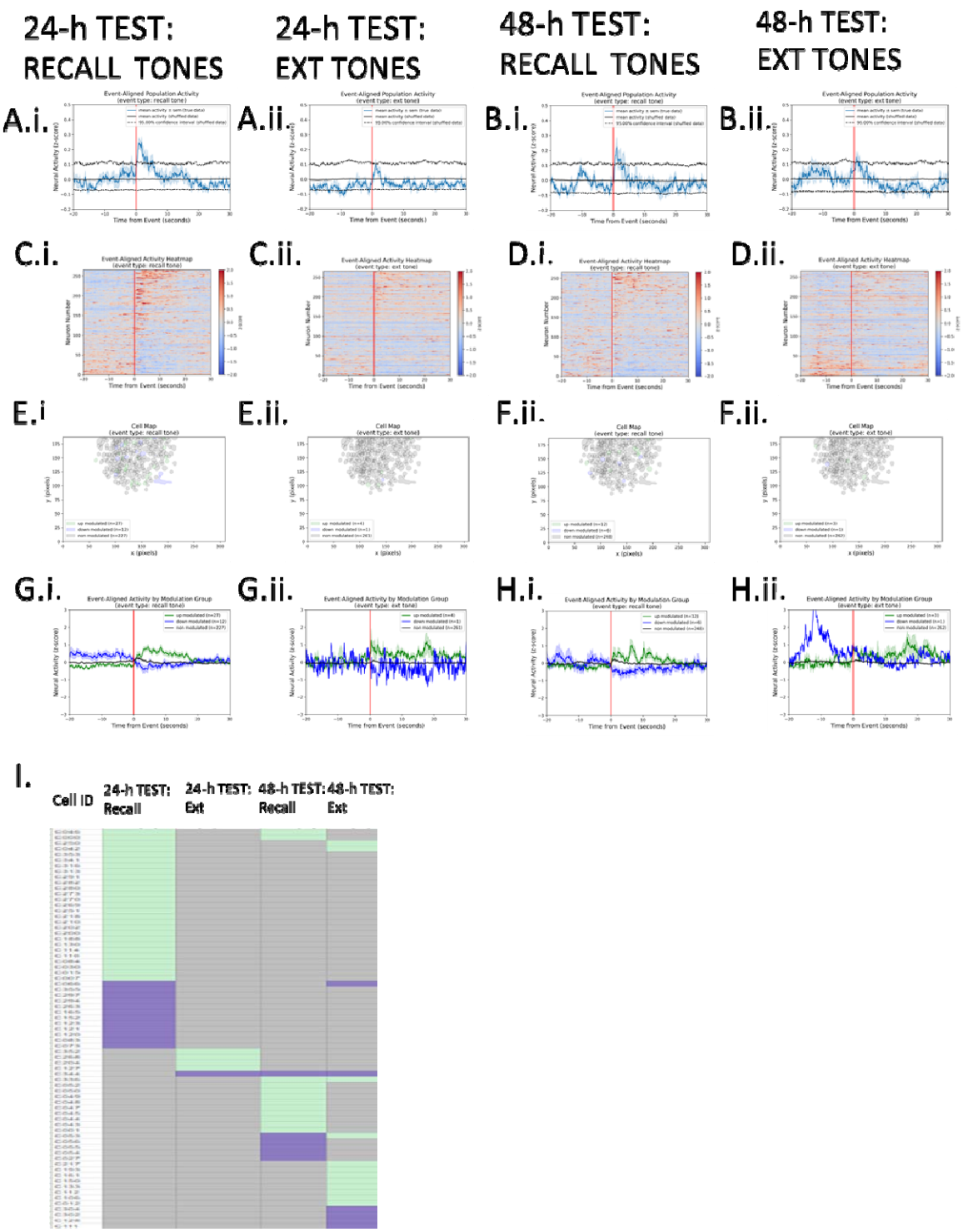

Supplementary Figure S6. Modulation of ACC activity in LR cell sets in response to the recall and extinction tones delivered during the 24-h and 48-h memory sessions from one representative subject.

A.i-A.ii: EAPA traces showing change of population activity over time in response to the recall (A.i) and extinction tones (A.ii) during the 24-h memory session. **B.i-B.ii:** EAPA traces showing change of population activity over time in response to recall (A.i) and extinction tones (A.ii) during the 48-h memory session. **C.i-C.ii:** Heatmaps of event-aligned neural activity for recall (C.i) and extinction tones (C.ii) during 24-h memory session. **D.i-D.ii:** Heatmaps of event-aligned neural activity for recall (D.i) and extinction tones (D.ii) during the 48-h memory session**.** **E.i-E.ii:** Cell maps representing the spatial distribution of neurons modulated by recall (E.i) and extinction tones (E.ii) during the 24-h memory session. **F.i-F.ii:** Cell maps representing the spatial distribution of neurons modulated by recall (E.i) and extinction tones (E.ii) during the 48-h memory session. **G.i-G.ii:** Event-aligned activity traces for up-modulated, down-modulated, and non-modulated neurons during recall (G.i) and extinction tones (G.ii) during the 24-h memory session. **H.i-H.ii:** Event-aligned activity traces for modulated subpopulations of neurons during recall (H.i) and extinction tones (H.ii) during the 48-h memory session. **I:** Heatmap showing individual neuron modulation states across all conditions (24-h recall, 24-h extinction, 48-h recall, 48-h extinction). Each row represents a neuron, and each column represents a condition. Cells are color-coded based on modulation status, revealing how the responses of individual neurons change across the different tones and sessions.

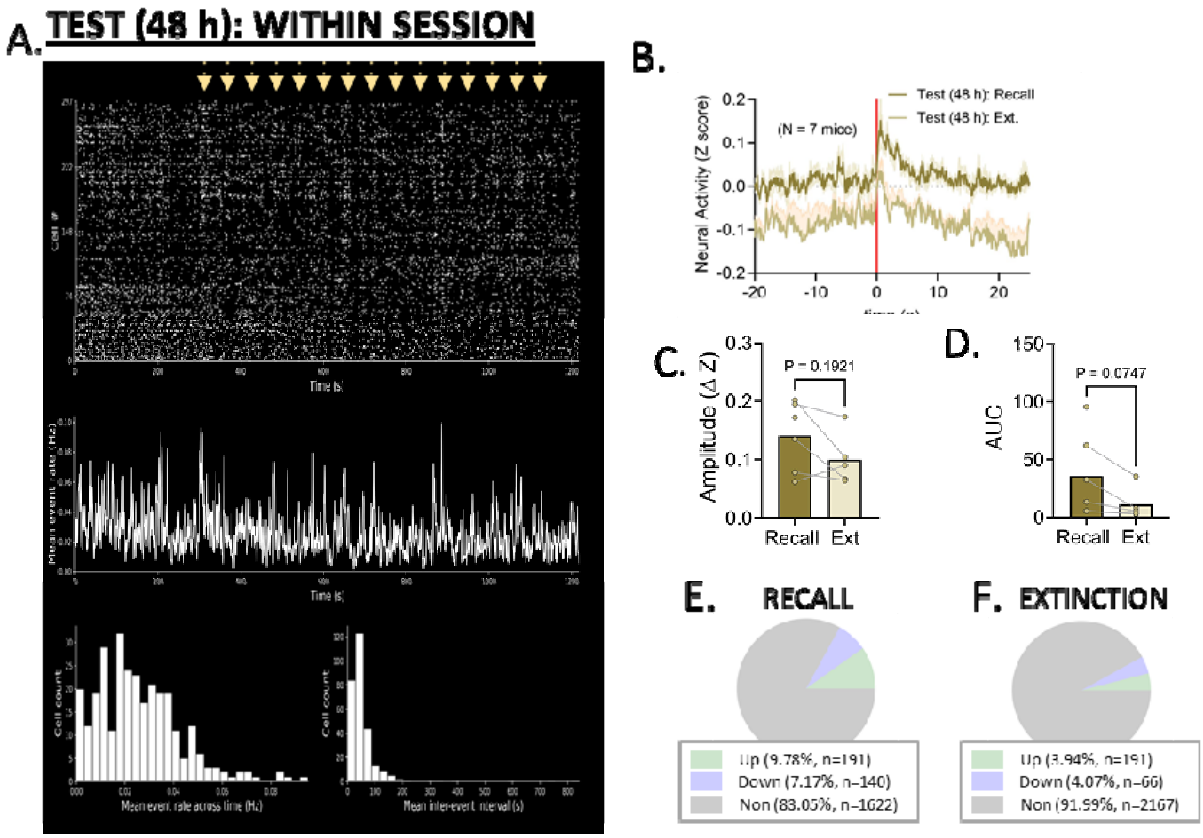

Supplementary Figure S7. ACC neural activity in response to recall and extinction tones during the 48-h memory session. **A-F: Within-session analysis. A:** Top: Raster plot showing neural activity during the 48-h memory session (yellow arrowheads indicate times of tone presentations). Middle: Average neural activity trace across all recorded neurons from the representative subject. Bottom: Histograms representing the distribution of mean event rates and mean inter-event intervals. **B:** Comparison of the event-aligned population activity traces during recall (dark olive) and extinction (light olive) tones during the 48-h memory session. **C-D:** Bar plots comparing amplitude (C) and AUC (D) for recall and extinction tones during the 48-h memory session. **E-F:** Pie charts showing the proportion of neurons modulated by recall tones (E) and extinction tones (F) during the 48-h memory session.

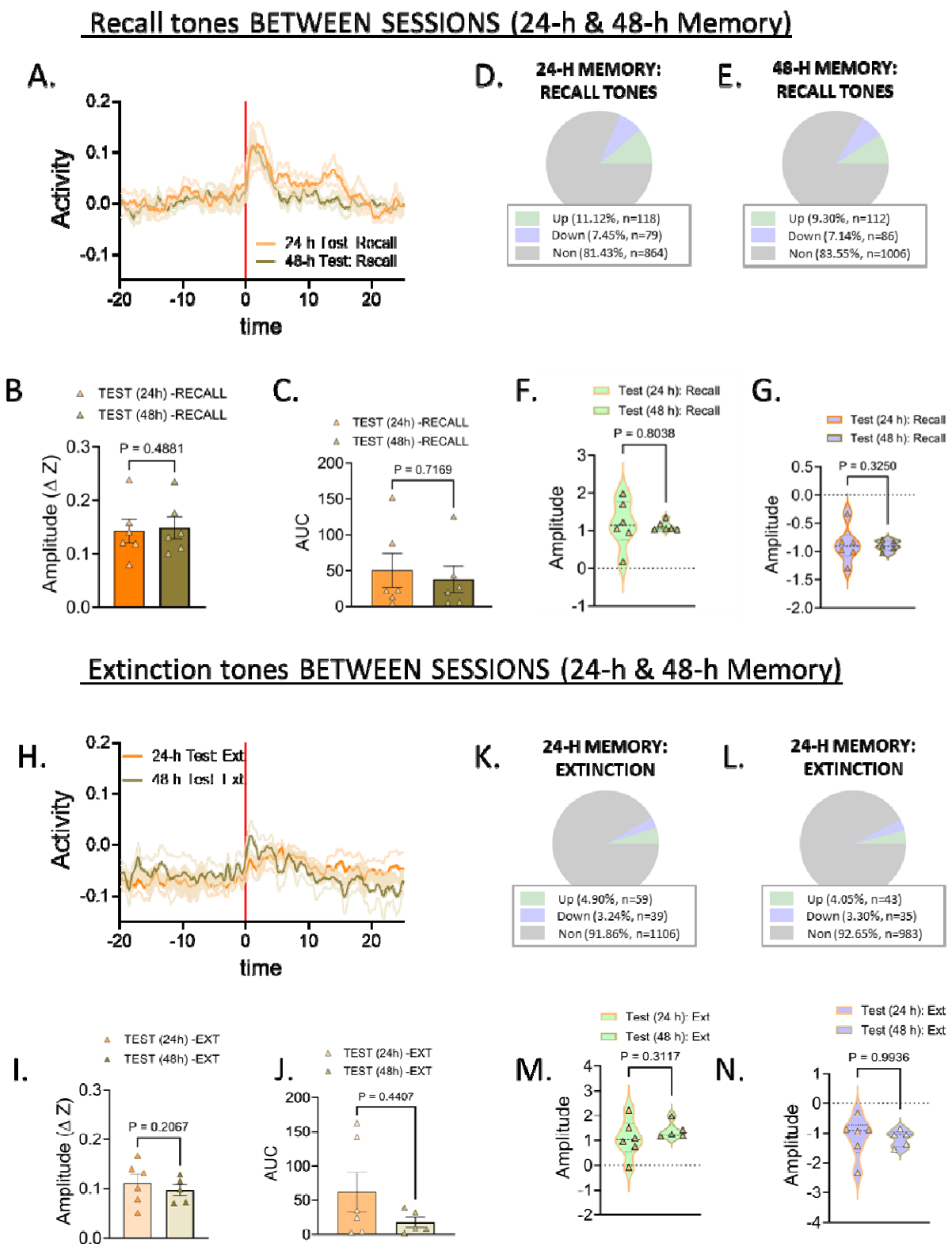

Supplementary Figure S8: Comparison of neural activity during recall and extinction tones between 24-h and 48-h memory sessions.

A-G: Recall tones between memory 24-h and 48-h memory sessions. (A) Mean population activity traces comparing neural responses to recall tones during the 24-h memory and 48-h memory sessions. (B-C) Bar plots comparing amplitude (B) and AUC (C) of neural activity between the 24-h and 48-h memory sessions during recall tones. Panel B: amplitude, 2-tailed T-test, p=0.49, t=0.75, N=6; Panel C: AUC, 2-tailed T-test, p=0.23, t=1.4, N =5. (D-E) The proportion of neurons modulated during recall tones for the 24-h memory (D) and 48-h memory (E) sessions. (F-G) Violin plots comparing the amplitude of up-modulated (F) and down-modulated (G) neurons during recall tones between the 24-hour and 48-h memory sessions. **H-N:** Extinction tones between 24-h and 48-h memory sessions. (H) Mean population activity traces comparing neural responses to extinction tones during the 24-h and 48-h memory sessions. (I-J) Bar plots comparing amplitude (I) and AUC (J) of neural activity between the 24-h and 48-h memory sessions during extinction tones. Panel I: paired t-test, p=0.2067, t=1.505, N=5; panel J, AUC (p=0.4407, t=0.8551, N=5. (K-L) Pie charts representing the proportion of neurons modulated during extinction tones for the 24-h memory (K) and 48-h memory (L) sessions. (M-N) Violin plots comparing the amplitude of up-modulated (M) and down-modulated (N) neurons during extinction tones between the 24-h and 48-h memory sessions. 2-tailed T test up-modulated cells: p=0.3117, down-modulated cells: p=0.9936.

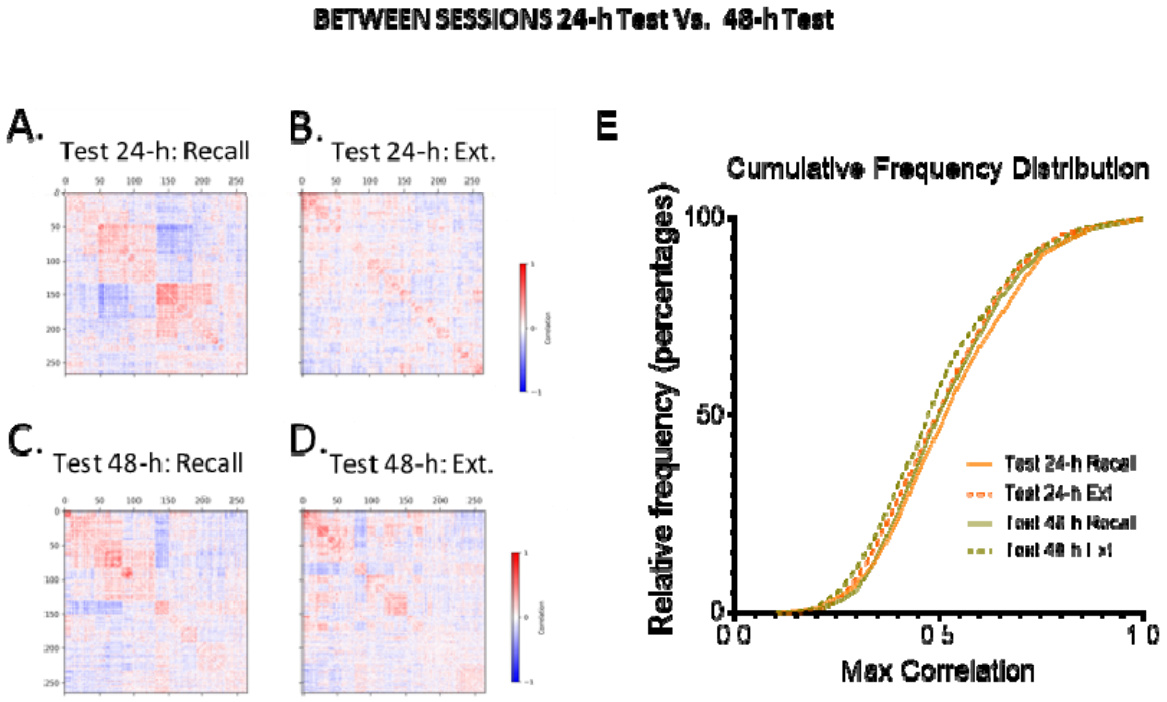

Supplementary Figure 9. Evolution of neural synchrony during the 48-h memory session.

A-D: Heatmaps of correlations between the 24-h memory (recall: panel A; extinction: panel B) and 48-h memory (recall: panel C; extinction: panel D) sessions. **E**: Cumulative frequency distribution of maximum correlations for 24-h and 48-h memory sessions (recall and extinction).

BIBLIOGRAPHY

1. A. L. Mahan, K. J. Ressler, Fear conditioning, synaptic plasticity and the amygdala: implications for posttraumatic stress disorder. *Trends Neurosci* **35**, 24-35 (2012).
2. W. H. Alexander, J. W. Brown, The Role of the Anterior Cingulate Cortex in Prediction Error and Signaling Surprise. *Top Cogn Sci* **11**, 119-135 (2019).
3. D. Wu *et al.*, Persistent Neuronal Activity in Anterior Cingulate Cortex Correlates with Sustained Attention in Rats Regardless of Sensory Modality. *Sci Rep* **7**, 43101 (2017).
4. E. T. Rolls, The mechanisms for pattern completion and pattern separation in the hippocampus. *Front Syst Neurosci* **7**, 74 (2013).
5. E. T. Rolls, The cingulate cortex and limbic systems for emotion, action, and memory. *Brain Struct Funct* **224**, 3001-3018 (2019).
6. E. Vassena, J. Deraeve, W. H. Alexander, Surprise, value and control in anterior cingulate cortex during speeded decision-making. *Nat Hum Behav* **4**, 412-422 (2020).
7. P. Feng, T. Feng, Z. Chen, X. Lei, Memory consolidation of fear conditioning: bi-stable amygdala connectivity with dorsal anterior cingulate and medial prefrontal cortex. *Soc Cogn Affect Neurosci* **9**, 1730-1737 (2014).
8. A. Pissiota *et al.*, Amygdala and anterior cingulate cortex activation during affective startle modulation: a PET study of fear. *Eur J Neurosci* **18**, 1325-1331 (2003).
9. H. Toyoda *et al.*, Interplay of amygdala and cingulate plasticity in emotional fear. *Neural Plast* **2011**, 813749 (2011).
10. S. Bissiere *et al.*, The rostral anterior cingulate cortex modulates the efficiency of amygdala-dependent fear learning. *Biol Psychiatry* **63**, 821-831 (2008).
11. M. A. X. de Lima, M. V. C. Baldo, F. A. Oliveira, N. S. Canteras, The anterior cingulate cortex and its role in controlling contextual fear memory to predatory threats. *Elife* **11** (2022).
12. I. Goshen *et al.*, Dynamics of retrieval strategies for remote memories. *Cell* **147**, 678-689 (2011).
13. C. J. Han *et al.*, Trace but not delay fear conditioning requires attention and the anterior cingulate cortex. *Proc Natl Acad Sci U S A* **100**, 13087-13092 (2003).
14. J. Jhang *et al.*, Anterior cingulate cortex and its input to the basolateral amygdala control innate fear response. *Nat Commun* **9**, 2744 (2018).
15. T. Kitamura *et al.*, Engrams and circuits crucial for systems consolidation of a memory. *Science* **356**, 73-78 (2017).
16. H. W. Steenland, X. Y. Li, M. Zhuo, Predicting aversive events and terminating fear in the mouse anterior cingulate cortex during trace fear conditioning. *J Neurosci* **32**, 1082-1095 (2012).
17. J. Tang *et al.*, Pavlovian fear memory induced by activation in the anterior cingulate cortex. *Mol Pain* **1**, 6 (2005).
18. P. W. Frankland, B. Bontempi, L. E. Talton, L. Kaczmarek, A. J. Silva, The involvement of the anterior cingulate cortex in remote contextual fear memory. *Science* **304**, 881-883 (2004).
19. E. O. Einarsson, K. Nader, Involvement of the anterior cingulate cortex in formation, consolidation, and reconsolidation of recent and remote contextual fear memory. *Learn Mem* **19**, 449-452 (2012).
20. S. Patel, K. Johnson, D. Adank, L. E. Rosas-Vidal, Longitudinal monitoring of prefrontal cortical ensemble dynamics reveals new insights into stress habituation. *Neurobiol Stress* **20**, 100481 (2022).
21. P. Zhou *et al.*, Efficient and accurate extraction of in vivo calcium signals from microendoscopic video data. *Elife* **7** (2018).
22. T. W. Chen *et al.*, Ultrasensitive fluorescent proteins for imaging neuronal activity. *Nature* **499**, 295-300 (2013).

23. M. E. Bowers, K. J. Ressler, Interaction between the cholecystokinin and endogenous cannabinoid systems in cued fear expression and extinction retention. *Neuropsychopharmacology* **40**, 688-700 (2015).
24. M. Fendt, M. S. Fanselow, The neuroanatomical and neurochemical basis of conditioned fear. *Neurosci Biobehav Rev* **23**, 743-760 (1999).
25. J. J. Kim, M. W. Jung, Neural circuits and mechanisms involved in Pavlovian fear conditioning: a critical review. *Neurosci Biobehav Rev* **30**, 188-202 (2006).
26. S. Maren, Neurobiology of Pavlovian fear conditioning. *Annu Rev Neurosci* **24**, 897-931 (2001).
27. K. Niikura *et al.*, Enhancement of glutamatergic transmission in the cingulate cortex in response to mild noxious stimuli under a neuropathic pain-like state. *Synapse* **65**, 424-432 (2011).
28. R. Zhao *et al.*, Neuropathic Pain Causes Pyramidal Neuronal Hyperactivity in the Anterior Cingulate Cortex. *Front Cell Neurosci* **12**, 107 (2018).
29. M. A. Acuna, F. Kasanetz, P. De Luna, M. Falkowska, T. Nevian, Principles of nociceptive coding in the anterior cingulate cortex. *Proc Natl Acad Sci U S A* **120**, e2212394120 (2023).
30. X. H. Li *et al.*, Activation of the glutamatergic cingulate cortical-cortical connection facilitates pain in adult mice. *Commun Biol* **6**, 1247 (2023).
31. B. Y. Hayden, S. R. Heilbronner, J. M. Pearson, M. L. Platt, Surprise signals in anterior cingulate cortex: neuronal encoding of unsigned reward prediction errors driving adjustment in behavior. *J Neurosci* **31**, 4178-4187 (2011).
32. J. R. Wessel, T. A. Klein, D. V. Ott, M. Ullsperger, Lesions to the prefrontal performance-monitoring network disrupt neural processing and adaptive behaviors after both errors and novelty. *Cortex* **50**, 45-54 (2014).
33. K. S. Gansel, Neural synchrony in cortical networks: mechanisms and implications for neural information processing and coding. *Front Integr Neurosci* **16**, 900715 (2022).
34. T. D. Marks, M. J. Goard, Stimulus-dependent representational drift in primary visual cortex. *Nat Commun* **12**, 5169 (2021).
35. C. E. Schoonover, S. N. Ohashi, R. Axel, A. J. P. Fink, Representational drift in primary olfactory cortex. *Nature* **594**, 541-546 (2021).
36. P. W. Frankland *et al.*, Stability of recent and remote contextual fear memory. *Learn Mem* **13**, 451-457 (2006).
37. Z. Albo, J. Graff, The mysteries of remote memory. *Philos Trans R Soc Lond B Biol Sci* **373** (2018).
38. J. L. McClelland, B. L. McNaughton, R. C. O'Reilly, Why there are complementary learning systems in the hippocampus and neocortex: insights from the successes and failures of connectionist models of learning and memory. *Psychol Rev* **102**, 419-457 (1995).
39. L. Nadel, A. Samsonovich, L. Ryan, M. Moscovitch, Multiple trace theory of human memory: computational, neuroimaging, and neuropsychological results. *Hippocampus* **10**, 352-368 (2000).
40. M. A. Fullana *et al.*, Fear extinction in the human brain: A meta-analysis of fMRI studies in healthy participants. *Neurosci Biobehav Rev* **88**, 16-25 (2018).
41. X. L. Bian *et al.*, Anterior Cingulate Cortex to Ventral Hippocampus Circuit Mediates Contextual Fear Generalization. *J Neurosci* **39**, 5728-5739 (2019).